Exploring the Structural, Dynamic, and Functional Properties of Metal-Organic Frameworks through Molecular Modeling

Filip Formalik, Kaihang Shi, Faramarz Joodaki, Xijun Wang, and Randall Q. Snurr*

This review spotlights the role of atomic-level modeling in research on metal-organic frameworks (MOFs), especially the key methodologies of density functional theory (DFT), Monte Carlo (MC) simulations, and molecular dynamics (MD) simulations. The discussion focuses on how periodic and cluster-based DFT calculations can provide novel insights into MOF properties, with a focus on predicting structural transformations, understanding thermodynamic properties and catalysis, and providing information or properties that are fed into classical simulations such as force field parameters or partial charges. Classical simulation methods, highlighting force field selection, databases of MOFs for high-throughput screening, and the synergistic nature of MC and MD simulations, are described. By predicting equilibrium thermodynamic and dynamic properties, these methods offer a wide perspective on MOF behavior and mechanisms. Additionally, the incorporation of machine learning (ML) techniques into quantum and classical simulations is discussed. These methods can enhance accuracy, expedite simulation setup, reduce computational costs, as well as predict key parameters, optimize geometries, and estimate MOF stability. By charting the growth and promise of computational research in the MOF field, the aim is to provide insights and recommendations to facilitate the incorporation of computational modeling more broadly into MOF research.

F. Formalik, K. Shi, F. Joodaki, X. Wang, R. Q. Snurr
Department of Chemical and Biological Engineering
Northwestern University
Evanston, IL 60208, USA
E-mail: snurr@northwestern.edu

F. Formalik
Department of Micro
Nano and Bioprocess Engineering
Faculty of Chemistry
Wroclaw University of Science and Technology
50-370 Wroclaw, Poland

K. Shi
Department of Chemical and Biological Engineering
University at Buffalo, The State University of New York
Buffalo, NY 14260, USA

1. Introduction

Reticular materials, such as metal-organic frameworks (MOFs) and covalent organic frameworks (COFs), have attracted significant attention over the past two decades due to their exceptional properties and diverse applications. These materials are characterized by their highly ordered porous structures, which can be precisely tailored to suit a wide range of applications, including gas storage,[1–4] separation,[5] and catalysis.[6–9] The field has seen considerable progress since the early years of the 21st century, with various research groups reporting the synthesis of unique materials. It is worth noting that the study of 3D coordination polymers dates back to the early 20th century, with the well-known example of Prussian blue,[10] but it was only in the late 1990s that such materials were synthesized with permanent porosity. In 2013 the International Union of Pure and Applied Chemistry (IUPAC) provided recommendations on the terminology that should be used in reticular chemistry research and defined a MOF as a coordination network with organic ligands containing potential voids.[11]

In this review, we explore the role of molecular modeling in MOF-related research, with a supplementary focus on how machine learning can augment traditional modeling techniques. By highlighting both the strengths and limitations of these approaches, we hope to inspire new avenues of research and development in this exciting area of materials science. Through the presentation of examples, we showcase the application of molecular modeling methods to tackle significant challenges in this field. In doing so, we aim to shed some light on the understanding of molecular modeling and machine learning techniques that can be used in MOF research, particularly for early-stage researchers and experimentalists who are seeking to enhance their grasp of these computational methodologies. Through relevant examples, we demonstrate the role of these techniques in addressing critical challenges and as a complementary tool to experiment in the discovery of new MOFs for particular applications.

The organization of this review is as follows: We begin with a historical perspective on the synthesis and modeling of MOFs, setting the context for the remainder of the discussion. Next, we

**ADVANCED
SCIENCE NEWS**

www.advancedsciencenews.com

**ADVANCED
FUNCTIONAL
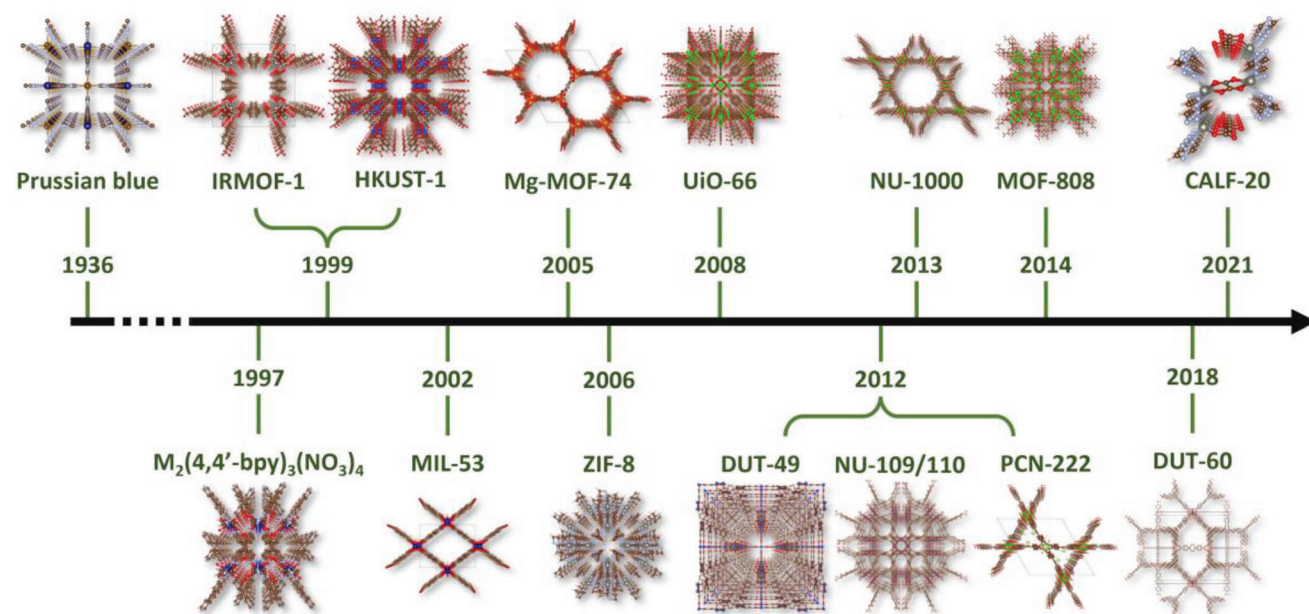MATERIALS**

www.afm-journal.de

Figure 1. Timeline highlighting some milestones in the synthesis of new MOFs, featuring their respective discovery years.

delve into density functional theory (DFT) and highlight several of its applications in studying MOFs. Subsequently, we explore how machine learning techniques can aid in executing DFT. We then shift our focus to classical methods, specifically molecular dynamics (MD) and Monte Carlo (MC) simulations, to examine thermodynamic and transport phenomena in MOFs, such as adsorption and diffusion. The review also provides some remarks on simulation choices for classical methods. Further, we explore the integration of machine learning techniques to enhance these classical methods. Finally, we conclude with a synthesis of the insights gained and a projection of future directions in the field.

2. Historical Overview

2.1. Historical Review of the Development and Synthesis of MOFs

In 1989, Hoskins and Robson pioneered the concept of creating solid, hybrid polymeric materials by interlinking metallic centers with tetrahedral or octahedral valency using rod-like organic linkers connectors, suggesting the potential for unique structures and large interconnected cavities.[12] In a noteworthy development in 1997, the group of Kitagawa introduced a framework with gas-adsorption capabilities at ambient temperature.[13] The properties of this framework allow it to be included in the modern definition of MOF. It is best described as a tongue-and-groove (bilayer) configuration, with the chemical formula $\{[M_2(4,4'\text{-bpy})_3(NO_3)_4] \cdot x\,H_2O\}_n$ (M = Co, x = 4; Ni, x = 4; Zn, x = 2, bpy = bipyridine). This structure is assembled from $M(NO_3)_2$ and 4,4'-bpy units. The pore sizes of the dehydrated sample are approximately 3 to 6 Å. This material showed the ability to reversibly adsorb CH_4, N_2, and O_2, as one of the earliest examples in the new era of nanoporous materials. The first occurrence of the term "metal-organic framework" in the litera-

ture was in a 1995 paper by Yaghi and Li.[14] In 1999, this same team reported the synthesis of MOF-5 (also known as IRMOF-1), which swiftly became one of the most extensively studied MOF structures.[15] In a follow-up paper, Yaghi and co-workers introduced the concept of isoreticular chemistry, allowing the systematic expansion of MOF structural design space through varying the organic linkers and the connectivity of inorganic nodes.[16] This was a landmark in the design and synthesis of new MOFs with customizable properties. Today, there are thousands of MOFs that have been reported in the literature, with more than 14000 frameworks deposited in the Computation-Ready, Experimental (CoRE) MOF database[17,18] (a more detailed discussion on the CoRE MOF database and other pivotal databases in the MOF research community is provided in Section 4.3.1). We discuss a few well-known MOFs from a historical perspective, as shown in **Figure 1**.

Cu-BTC, also known as HKUST-1 or MOF-199, was reported in 1999 by Chui et al. at the Hong Kong University of Science and Technology (HKUST).[19] This framework was presented as a material with high surface area and exceptional gas adsorption properties, making it a widely studied material for various applications, including gas storage and separation. Synthesis of another important framework, Mg-MOF-74 (also known as CPO-27-Mg),[20] focused research attention on the concept of an open metal site (OMS), which is a coordinatively unsaturated metal node in a MOF that is accessible to guest molecules. OMS enables enhanced chemical interactions that can significantly influence the adsorption of various gases, including those with dipolar, quadrupolar, and other distinct molecular characteristics. These sites can also serve as catalysts. The magnesium OMS in Mg-MOF-74 demonstrates a notable contribution to the high gas adsorption capacities of this framework, particularly for quadrupolar carbon dioxide (CO_2) and other gas molecules that can engage in strong chemical interactions. Moreover, the MOF-74 structure offers the flexibility

to incorporate diverse transition metals, enabling the fine-tuning of its adsorption and catalytic properties and making this a platform material for many investigations. Similar to IRMOF-1, isoreticular versions of MOF-74 have been synthesized by increasing the linker size. As a result, a MOF boasting some of the largest pore sizes ever recorded (exceeding 70 Å) was successfully synthesized.[21]

The discovery of MIL-53 (MIL = Materials Institute Lavoisier), reported by Gérard Férey and his team in 2002,[22] marked a significant milestone by extending MOF chemistry to include trivalent Cr^{III} metal ions. In 2004, they showed that the isoreticular Al^{III} variant of this MOF exhibits framework flexibility in response to external stimuli.[23] MIL-53 along with its isoreticular but less flexible counterpart, MIL-47(V^{IV})[24], shows the ability to undergo reversible structural transitions, often referred to as *breathing* behavior, in response to changes in temperature, pressure, or the presence of guest molecules. The breathing behavior of MIL-53 is attributed to the rotation of its organic linkers, which changes the steric hindrance in its structure and allows the framework to adopt two distinct phases: a narrow-pore phase (MIL-53(np)) and a large-pore phase (MIL-53(lp)). The transition between these phases is accompanied by significant changes in the unit cell volume from 890 to 1430 Å.[25]

Another important class of MOFs are the zeolitic imidazolate frameworks (ZIFs), which share structural similarities with zeolites and were introduced in 2006 by Huang et al.[26] Whereas zeolites are built from Si-O-Si linkages with a bond angle of about 145°, ZIFs are built from M-Im-M linkages, where M is typically a metal cation in the 2^+ oxidation state and Im is a derivative of an imidazolate anion, which serves as a linker (imidazolate, methylimidazolate, nitroimidazolate, etc.). In 2006, Yaghi and co-workers reported the synthesis of a set of 12 ZIFs with various zeolitic topologies.[27] ZIF-8, an extensively studied ZIF structure, demonstrated exceptional chemical stability (7 days in boiling water; 24 h in aqueous sodium hydroxide at 100°C) and thermal stability (up to 550 °C, in N_2 atmosphere). ZIF-8′s stability, combined with its high surface area and tunable chemistry, has led to its extensive study for gas storage and separation applications. ZIF-8 is also considered a flexible MOF due to the gate-opening phenomenon it undergoes. In this deformation, imidazolate linkers of a 6-member ring rotate and increase the pore-limiting diameter (PLD) when exposed to the flow of adsorbate (N_2)[28] and external hydrostatic pressure (1.5 GPa).[29]

Another subgroup of materials with high stability are Zr-MOFs, which are distinguished by the presence of Zr_6O_8 metal nodes within their structures. The first synthesized framework from this group, UiO-66, was reported in 2008 by Lillerud and co-workers at the University of Oslo, Norway, which inspired its name (UiO = *Universitetet i Oslo*).[30] This MOF is composed of 12-connected zirconium oxide nodes connected by 1,4-benzenedicarboxylate (BDC) linkers. Due to its high thermal (540°C, in N_2 atmosphere) and chemical stability (water and acid stability), UiO-66 and its derivatives have been extensively studied for various applications, including gas storage, separation, catalysis, and sensing. The discovery of UiO-66 as the 1st member of the Zr-MOF family has had a substantial impact on the development of new frameworks, making it an important milestone in the history of these materials. Another widely studied Zr-MOF, NU-1000, was synthesized in 2013 by Omar Farha and Joseph Hupp at Northwestern University (NU).[31] It contains 1D channel-like hexagonal mesopores and trigonal micropores and, like most of the Zr-MOFs, it shows high thermal and water stability. Unlike UiO-66, the metal node in NU-1000 is connected by 8 linkers, leaving 4 Lewis acid sites accessible. This results in various versions of this framework that differ by a chemical modulator attached to the node (such as aquo-hydroxo pairs, formate, acetate, trifluoroacetate, metal atoms, and oxides, etc.), which can significantly alter its properties (such as level of hydrophilicity or catalytic activity).[32] The chemically labile nature of the node makes it also an interesting candidate as a catalyst for many important reactions, such as the decomposition of nerve agents.[33] Another important Zr-MOF, MOF-808, was reported in 2014 by the Yaghi group.[34] It has 6-connected nodes and has been shown as a promising candidate for water adsorption (e.g., for water harvesting applications) due to its relatively high uptake at low relative humidity.[34] The final Zr-MOF discussed here is PCN-222 and was synthesized by Hong-Cai Zhou at Texas A&M University in 2012.[35] This is a mesoporous MOF, isoreticular with NU-1000, that displays biomimetic catalytic activity. The catalytically active site is a Fe-porphyrin complex, which is incorporated into the linker situated on the inner wall of an open channel with a 37 Å diameter. The material demonstrates good activity for oxidizing various substrates. The combination of a high density of catalytic centers, ultra-large open channels (for MOF standards), and exceptional chemical stability of PCN-222(Fe) indicate great potential for creating MOF-based platforms for enzyme-mimicking catalysis.

The group of Stefan Kaskel from the Dresden University of Technology (DUT) contributed to the field of reticular materials chemistry with a range of frameworks. Particularly interesting is DUT-49 (synthesized in 2012), which demonstrates the peculiar phenomenon of negative gas adsorption (NGA),[36,37] a rare behavior in which the adsorbed gas amount decreases with increasing pressure under certain conditions. This unusual property is attributed to a structural change in the MOF, which involves a transition between two different pore sizes and is induced by strong adsorbent-adsorbate interactions.

MOFs are renowned for their exceptionally high surface areas (SA), which can exceed that of other porous materials such as zeolites and activated carbons. MOF-5, introduced in 1999, has a surface area of 3500 m^2 g^{-1}.[38] NU-110, a MOF synthesized in 2012 held the record for the highest surface area material (7140 m^2 g^{-1})[39] until 2018 when it was surpassed by DUT-60 (7800 m^2 g^{-1}).[40]

More recently, the MOF CALF-20 has attracted much attention. While the initial patent application was filed in 2014, the material was comprehensively characterized in terms of structure and properties by Shimizu and co-workers from the University of Calgary in Canada in 2021.[41] CALF-20 is a promising MOF for post-combustion CO_2 capture, as it meets the essential criteria for an ideal adsorbent, such as high CO_2 adsorption capacity, fast kinetics, high CO_2 selectivity, and stability under various conditions. Unlike many MOFs, CALF-20 can tolerate ambient moisture or steam, and its synthesis is cost-effective and scalable, using commercially available components and environmentally friendly solvents.
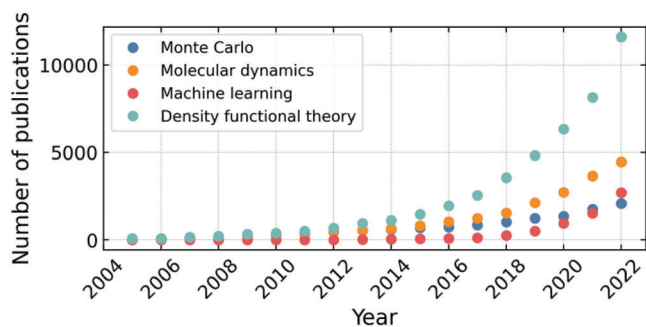
2308130 (3 of 25)

Figure 2. Trends in the utilization of various modeling techniques within the MOF field: a quantitative analysis based on publication count from Google Scholar (numbers represent publications per year). The data was extracted with an academic paper word occurrence tool.[42]

2.2. Historical Review of Molecular Modeling for MOFs

Throughout the history of MOFs, molecular modeling has played an important role in advancing our understanding of these materials (**Figure 2**). Computational methods have helped researchers predict the properties of MOFs, such as their adsorption capabilities or catalytic activity. These predictions have informed the design and synthesis of new materials, accelerating the discovery of novel structures with improved performance. Molecular modeling has also facilitated our understanding of the underlying mechanisms behind unique phenomena in MOFs, such as their remarkable structural flexibility and tunable pore environments. Over the years, numerous molecular modeling techniques have been employed to study reticular materials, including density functional theory (DFT), ab initio molecular dynamics (AIMD), and methods based on classical mechanics and statistical mechanics such as molecular dynamics (MD) and Monte Carlo (MC) simulations. These approaches have been instrumental in elucidating the structural and dynamic properties of MOFs and their interactions with various guest molecules.

The first articles reporting adsorption simulations in MOFs emerged in the early 2000s. In 2001, Kawakami et al.[43] utilized multiscale modeling, incorporating force fields and DFT, to explore the adsorption of magnetic and nonmagnetic species in a ZnBDC MOF. The authors highlighted the potential of nanoporous crystalline materials, such as MOFs, to serve as frameworks for controlling the distribution and orientation of absorbed molecular species due to their highly ordered structure. In 2003, the group of Alexander Neimark investigated argon adsorption in HKUST-1 using the grand canonical Monte Carlo (GCMC) method and reported an excellent agreement of the simulated and experimental adsorption isotherms.[44] They were able to identify preferential adsorption sites in the pores of the MOF based on the simulation snapshots. This highlights a crucial objective of molecular modeling: to complement experimental techniques by offering atomistic-level insights into phenomena that would otherwise be challenging through experimental methods alone. The use of extensive quantum-chemistry calculations in MOF-related research was featured in a significant study published in 2004,[45] where Sagara et al. used periodic DFT to optimize and derive partial charges for IRMOF-1 for subsequent GCMC adsorption simulations of H_2. Fragments of MOFs were

also selected to study the interaction energy of the framework with hydrogen molecules at the MP2 level of theory.

Düren et al. investigated the applicability of materials from the IRMOF family for methane storage using MC simulations[46] and proposed new, in-silico-designed isoreticular MOFs which maximized predicted methane uptake, demonstrating the effectiveness of simulations in guiding material design for various storage applications and paving the way for hypothetical MOF design. In another early study, Sarkisov et al. used molecular simulation to understand the properties of IRMOF-1 by exploring the adsorption and diffusion of methane, normal alkanes, cyclohexane, and benzene in this material.[47] Both studies underscore the usefulness of molecular simulations in understanding the properties of MOFs and guiding the design of new materials for adsorption applications, such as methane storage and separation processes. The diffusion of light gases (Ar, CH_4, CO_2, N_2, H_2) in IRMOF-1 was also studied by the group of Skoulidas and Sholl.[48] The results supported the idea that MOF diffusion coefficients are similar to those in zeolites, implying that experimental techniques used for zeolites should also be applicable to MOFs.

In 2009, Keskin and Sholl reported one of the first computational screening studies performed on eight frameworks aimed at finding MOF membranes for gas separation (CO_2/CH_4, CH_4/H_2, CO_4/H_2).[49] This number is modest when compared with the articles published nowadays that report simulation results for many hundreds or even thousands of structures. However, this early work laid the groundwork for contemporary large-scale screening simulations. In 2011, Wilmer et al. presented an extensive screening study on over 130 000 hypothetical MOFs.[50] They developed a computational approach to generate potential MOFs using a library of building blocks derived from known MOF structures. The attributes of each MOF, including pore-size distribution, surface area, and methane-storage capacity, were calculated. The study led to the identification of over 300 hypothetical MOFs with a predicted methane storage capacity superior to any known material and uncovered important structure-property relationships in the process. The large amount of data generated in such screening studies, together with the development of machine learning (ML) methods, has opened new opportunities for their application in the study of MOFs. The early work from Woo et al. demonstrated that by using machine learning with structural descriptors it is possible to quickly identify high-performing MOFs for CO_2 capture, reducing the need for compute-intensive screening and making the exploration of vast search spaces feasible for various applications.[51] The basics of machine learning methods and their applications to the discovery and design of porous materials have been discussed in several excellent reviews (e.g., ref.[52]).

3. First-Principles Computational Methods Applied to Reticular Materials

DFT is a computational method for approximating the solutions to the Schrödinger equation, the fundamental equation of quantum mechanics. For a given arrangement of atoms, DFT allows for the calculation of the energy, enabling the search for configurations that minimize the energy, as well as the identification of saddle points (energy barriers) on the potential energy surface. The method can provide information on the electronic
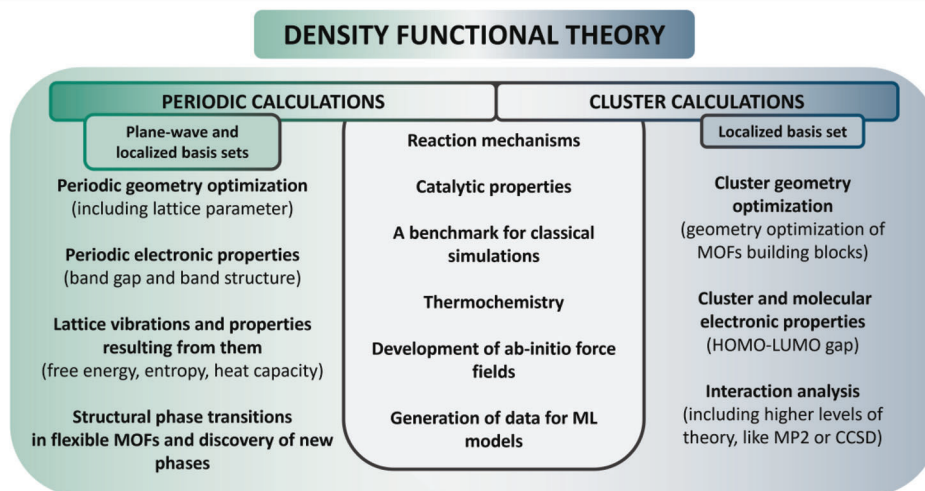
Figure 3. Applications of DFT calculations in the field of MOFs.

structure of atoms, molecules, and materials (**Figure 3**). DFT is rooted in the Hohenberg-Kohn theorems,[53] which establish that the ground-state properties of a many-electron system are uniquely determined by its electron density. Thus, in contrast to methods such as Hartree-Fock and its derivatives, which require solving the Schrödinger equation for a multitude of interacting electrons, DFT simplifies the computational task significantly by considering the energy of the system to be a functional of the electron density alone. An essential development in the practical application of DFT is the Kohn-Sham equations.[54] Introduced by Walter Kohn and Lu Jeu Sham, these equations present a method for converting the complex many-body problem into a set of single-particle equations. In the Kohn-Sham approach, the many-electron system is represented as a system of non-interacting electrons (an auxiliary system) that have the same ground state electron density as the actual system. Each electron in this auxiliary system moves in an effective potential, consisting of the classical electrostatic potential due to the nuclei and the other electrons, but this effective potential only considers the other electrons in a mean-field sense. In addition, the electrons experience what is known as the exchange-correlation potential, which encompasses the complex effects of electron-electron interactions. Unfortunately, this exchange-correlation functional is not known exactly, and approximations must be made. Solving these equations yields a set of Kohn-Sham orbitals and their energies, which provide valuable information about the electronic structure of the system.

When using DFT, the user must make several crucial decisions related to the approximations that will be made. First, the user must choose an appropriate exchange-correlation functional. There are many families of functionals, including local density approximations (LDA), generalized gradient approximations (GGA), and hybrid functionals, each with its strengths and weaknesses, computational cost, and applicability to certain problems. Second, the user must select a basis set, which is a set of functions used to expand the Kohn-Sham orbitals. Choosing a basis set is a trade-off between computational cost and accuracy. Larger basis sets provide more accurate results but at a higher

computational cost.[55] We refer the interested reader to standard textbooks on DFT for further detail.[56,57]

DFT has proven to be a valuable computational tool for studying a wide range of materials, including reticular materials such as MOFs. In practice, DFT calculations can be performed using two main approaches: plane wave basis functions and localized orbital basis sets. The plane wave approach represents the wavefunction and orbitals as a superposition of periodic plane waves, which is naturally suitable for studying periodic systems. Historically, it was applied to such systems as metals, semiconductors, or metal oxides and was most popular among physicists to study the structural and electronic properties of materials. On the other hand, the localized orbital approach employs a set of atom-centered basis functions (such as Gaussian or Slater functions) which are finite in extent and localized around atomic nuclei. This approach is more appropriate for non-periodic systems and was usually applied by computational chemists to study the properties of molecules.[55] Each of these two DFT approaches has its own strengths and limitations, depending on the nature of the system being studied and the specific scientific questions being addressed. MOFs, being periodic crystals but composed of discrete metal nodes and linkers, may be considered a kind of hybrid between molecular systems and classical periodic solids. Thus, both methods have been successfully applied in computational studies of MOFs. Figure 3 provides an overview of how DFT calculations within both approaches can be helpful in calculations and simulations for studying the use of MOFs in energy-related applications.

3.1. Geometry Optimization

Often, the first task in understanding a system is to obtain its lowest energy geometry. This can also be useful in preparing MOF structure for further simulations (either quantum mechanical or classical). Thus, optimizing the geometry of a MOF structure is often done by minimization of the energy and/or forces using DFT. While it is difficult to suggest the exchange-correlation (XC)
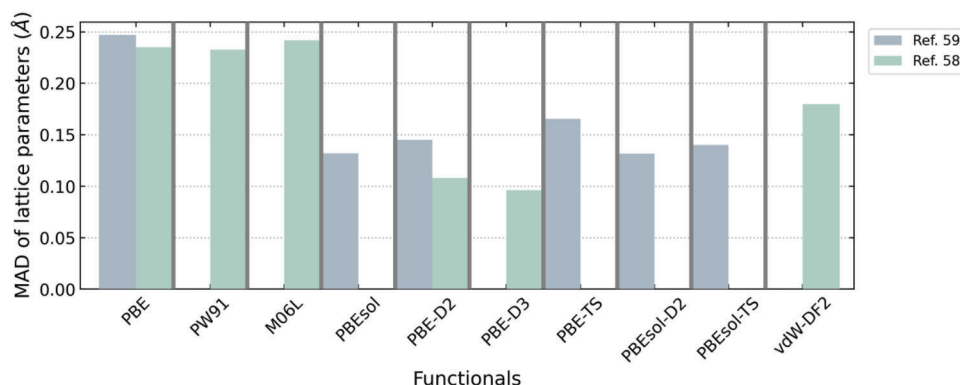
**ADVANCED
SCIENCE NEWS**

www.advancedsciencenews.com

**ADVANCED
FUNCTIONAL
MATERIALS**

www.afm-journal.de

Figure 4. Accuracy of density functionals in predicting lattice parameters of MOFs. Data taken from refs.[59,58] MAD is the mean absolute deviation of the lattice parameters.

functional that guarantees the highest accuracy, some groups have reported benchmark analysis based on a comparison of some structural properties derived from DFT calculations, such as lattice parameters, bond lengths, angles, and dihedrals in comparison to experimental data.[58,59] The authors emphasized that while no single XC functional consistently outperformed others, the selection of a functional should take into account the specific characteristics of the MOFs (such as flexibility) under study. They also strongly emphasized the importance of including long-range dispersion interactions in DFT calculations, either through empirical corrections (Grimme methods,[60–63] available in most periodic and cluster DFT codes or the Tkatchenko-Sheffler method[64]) or non-local van der Waals density functionals (vdW-DF).[65–69] Including dispersion interactions is needed to predict the correct structural phase for some flexible frameworks such as MIL-53 or ZIF-4. A summary of the discussed results is presented in **Figure 4**.

Flexibility in MOFs is related to collective lattice vibrations, known as phonons. Phonons extend the notion of local vibrational modes and provide insight into structural deformations. By analyzing phonons, one can anticipate how the material will react to temperature changes. The vibrations of the atoms in the lattice can contribute to structural changes or even the collapse of the MOF structure under certain conditions. Understanding phonon behavior in MOFs can help analyze or design materials with desired mechanical properties such as gate-opening,[70–74] breathing,[75,76] structural stability,[77] and negative thermal expansion.[78] Phonon modes can also affect the diffusion of gases in the pores through collective motions of the atoms in bottlenecks in the pore structure.[79]

3.2. Energetic Landscape of Flexible MOFs

Calculations of energy-volume relations can provide valuable insights into the structural deformations of MOFs, particularly when they incorporate information related to external stimuli. These calculations enable a deeper understanding of MOF response to various conditions, including temperature, pressure, and presence of guest molecules. Energy-volume relations describe the dependence of a material's energy on its volume, reflecting the interplay between internal forces and structural

changes. By analyzing these relations in MOFs, it is possible to gain insight into i) elastic properties such as bulk modulus, shear modulus, and Young's modulus, which are essential for predicting and optimizing MOF mechanical stability and resilience under different conditions[80,81]; ii) structural transitions through discovery and description of various phases, such as breathing in MIL-53,[82–84] negative thermal expansion in DUT-49,[85] pore opening transformation in JUK-8,[84,86] and contraction in CUK-1.[87]

In many cases, the energy-volume profile describes the Helmholtz free energy F with contributions from vibrational internal energy and vibrational entropy:

$$F(T, V) = E_{DFT}(V) + E_{vib}(T, V) - TS_{vib}(T, V) \qquad (1)$$

where E_{DFT} is the DFT energy (with dispersion contribution), E_{vib} is the vibrational internal energy (or harmonic phonon energy), S_{vib} is the vibrational entropy, and T and V represent temperature and volume, respectively. All contributions can be derived directly from the phonon partition function which can be obtained using frequencies of phonon modes[88] and applied to calculate the thermal dependency of the minimum-energy volume of a framework through the quasi-harmonic approximation.[89] **Figure 5** illustrates the energy versus volume relationships for three MOFs (MIL-53, DUT-49, and JUK-8), thereby shedding light on the structural phase transitions they undergo in response to varying external stimuli. In the case of MIL-53, a breathing transition is induced by temperature changes, stabilizing the structure in the np phase at lower temperatures (global minimum on the red curve), and transitioning to the lp phase as temperatures rise (global minimum on the blue curve). DUT-49 exhibits NGA where, due to interactions with guest molecules, the system contracts, transitioning from the open phase when empty (minimum of the red curve) to the closed phase when the number of guest molecules exceeds some threshold (minimum of the blue curve). JUK-8 undergoes a pore opening transition from a closed phase (minimum on the red curve) to an open phase (global minimum on the blue curve) when exposed to a specific pressure from guest molecules. These examples underscore the usefulness of energy versus volume relations in the analysis of structural phase transitions in MOFs.
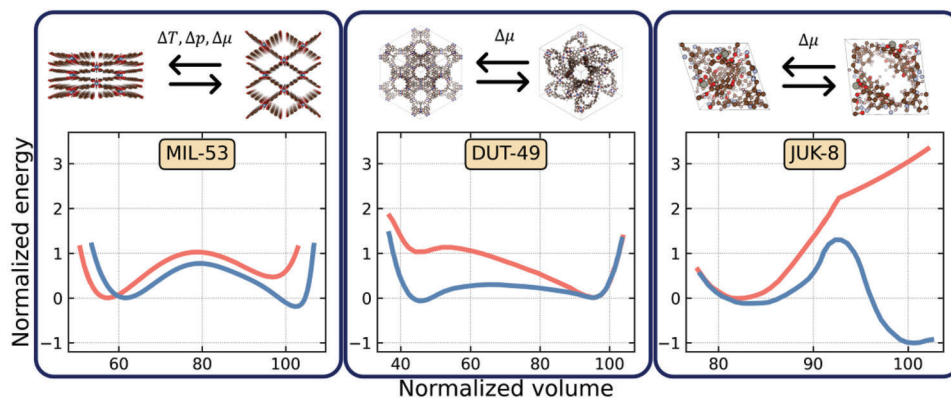
ADVANCED
SCIENCE NEWS
www.advancedsciencenews.com

ADVANCED
FUNCTIONAL
MATERIALS
www.afm-journal.de

Figure 5. Schematic free energy profiles that explain structural phase transitions: breathing in MIL-53, NGA in DUT-49, and pore-opening in JUK-8. The red lines represent free energy without the contribution of any stimulus (temperature, pressure, chemical potential); the blue lines represent the free energy under the influence of temperature (MIL-53, narrow to large pore transition), number of guest molecules present in the pores (DUT-49, large to contracted pore transition), and pressure of adsorbate (JUK-8, formation of new stable phase). Data taken from refs.[82,84,85]

3.3. Interactions of MOFs with Guest Molecules

DFT methods have proven to be valuable tools in examining the interactions of guest molecules with MOFs, especially when there are strong and specific chemical interactions beyond weak physisorption. As highlighted in the introduction, MOFs with Zr_6O_8 nodes are promising materials for many potential applications, including carbon capture and water harvesting, and interactions of these molecules with zirconium nodes exhibit interesting and sometimes unexpected behavior. Grissom et al. studied this problem by performing systematic infrared spectroscopic studies, which together with DFT calculations[90] showed that CO_2 adsorption in UiO-66 involves two main binding processes: hydrogen bonding with μ_3-OH groups inside the tetrahedral pores and through more typical dispersive interactions. The enthalpy of adsorption for hydrogen-bonded and dispersion-stabilized CO_2 species was found to be −38.0 and −30.2 kJ mol^{-1}, respectively. This example highlights how comparing calculated and measured infrared frequencies can be a useful method to validate computationally predicted host-guest interactions. The authors showed that different adsorption modes are related to different frequencies of CO_2 asymmetric stretching mode, with stronger interaction associated with larger redshift relative to bulk CO_2 (10 and 14 cm^{-1} for dispersion-stabilized and bonding with μ_3-OH groups, respectively). This can be explained by the effect of charge transfer between the CO_2 oxygen atom and the adsorbent, causing a weakening of the C—O bond and reducing the associated vibrational frequency (in the harmonic approximation, the energy is a linear function of the frequency). Potential binding of CO_2 on open metal sites in Zr-MOFs associated with missing linker defects was also predicted by DFT calculations, with an even higher adsorption enthalpy of -57 kJ mol^{-1}.

In a related study, Rayder et al. examined CO_2 adsorption on the 6-connected Zr node of MOF-808.[91] They discovered that changing the modulator attached to the node can induce monodentate binding, deviating from the usual bidentate binding (**Figure 6**). Monodentate binding opens up a Zr site for possible CO_2 chemisorption. The frequency shift of the stretching mode of chemisorbed CO_2, as calculated using DFT, aligned well with the experimental results. Tan et al. highlighted a similar

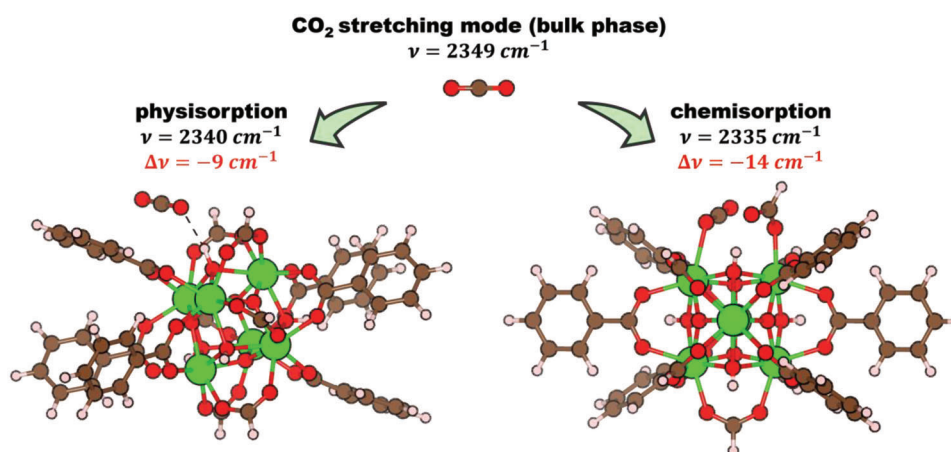**Figure 6.** Change of CO_2 stretching mode frequency calculated by DFT for MOF-808. Comparison of calculated and measured frequencies provided an explanation of the adsorption mechanism observed in experimental infrared spectroscopy. The frequencies taken from the ref.[91] Carbon atoms are brown, hydrogen white, oxygen red, zirconium green.

© 2023 The Authors. Advanced Functional Materials published by Wiley-VCH GmbH

**ADVANCED
SCIENCE NEWS**

www.advancedsciencenews.com

**ADVANCED
FUNCTIONAL
MATERIALS**

www.afm-journal.de

phenomenon[92] and based on the observation of a significant infrared band in the 1700–1650 cm^{-1} range of experimental spectra, they proposed a new perspective on defect termination in the MOF UiO-66. With periodic DFT calculations, they suggested the presence of unidentate COO$^-$ groups from the formate modulators stabilized by H-bonding with a terminal water molecule. Contrary to the assumption that modulator COO$^-$ groups bind tightly with two Zr sites via bidentate coordination, it was shown that water readily inserts and breaks one of the Zr—O—C bonds, forming a detectable C=O absorption band above 1650 cm^{-1}. The high catalytic activity observed in defective UiO-66 may be attributed to its ability to easily add and remove water molecules.

Vibrational frequencies calculated by DFT may show systematic deviations from experimental values, and this is typically addressed through the application of an empirical scaling factor. One way to obtain the scaling factor is to take the ratio of a well-known, relevant experimental frequency (like the bulk CO$_2$ stretching mode at 2349 cm^{-1}) to the calculated DFT value. Alternatively, one can consider using a database of scaling factors developed by the group of Truhlar[93,94] (note that there are different scaling factors for comparing infrared frequencies with experiment and for thermochemistry).

The evaluation of interaction energies typically necessitates the calculation of both the enthalpy and free energy associated with the process. They are typically obtained from thermal energies and entropies. The contributions from low frequencies introduce significant noise when applying the rigid-rotor harmonic approximation (as the vibrational entropy asymptotically reaches infinity when frequencies approach 0). To overcome this limitation, a quasi-rigid-rotor-harmonic-approximation (quasi-RRHO) was proposed by Stefan Grimme, in which, for the frequencies lower than the selected cutoff (usually between 50 and 150 cm^{-1}), the entropy is calculated as the combination of vibrational and rotational entropies.[95] For systems containing more than 300 atoms, this approach can change the free energies up to 15 kJ mol^{-1}. Similar improvement is observed when the quasi-RRHO approximation is applied in adsorption enthalpy calculations,[96] which are of great interest in the MOF simulation community. Moreover, when using an implicit solvent model or considering various configurations of reacting species, it is crucial to also account for solvation and configurational entropies.[95,97] GoodVibes is a versatile Python tool that calculates thermochemical data from quantum chemistry calculations, accounting for all the issues described in this paragraph. With automated features, it saves researchers time, incorporates valuable corrections, and prevents human errors in analyzing large numbers of output files.[98]

3.4. Catalysis

DFT has emerged as a powerful tool for studying and predicting the catalytic behavior of MOFs, as well as unraveling the intricate structure-property relationships that underlie catalytic processes. In a typical application, the researcher postulates a set of reaction intermediates and tries to optimize their geometries using DFT. Then, saddle points connecting the intermediates are located to provide the transition states and the energy barriers for the proposed reaction mechanism. For example, **Figure 7** shows a simple reaction pathway for the MOF-catalyzed hydrol-
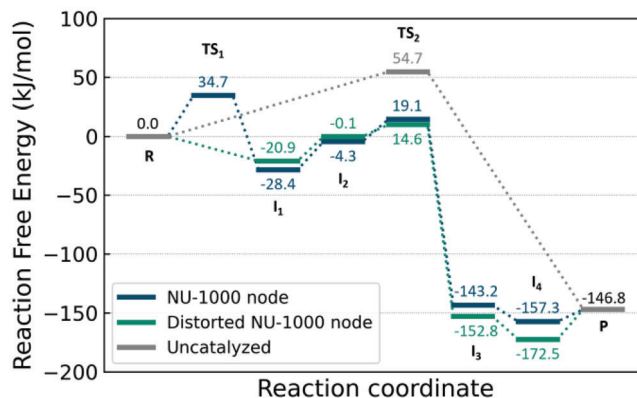

Figure 7. Free energy diagram for reaction pathway of DMNP hydrolysis using two types of Zr clusters in NU-1000 MOF, compared to the uncatalyzed scenario. Figure recreated based on the data from ref.[99] R—reactant, TS—transition state, I$_n$—intermediate state, P—product.

ysis of the chemical warfare agent simulant DMNP, as well as the uncatalyzed reaction.[99] The free energy diagram illustrates that the barrier for the MOF-catalyzed reaction associated with the transition state TS$_2$ (measured as the free energy difference between TS$_2$ and the intermediate I$_1$) is significantly lower than that of the uncatalyzed reaction (measured as the free energy difference between TS$_2$ and R). Additionally, the reaction free energy diagram shows that in the distorted node, the 1st transition state TS$_1$ (related to the dehydration of the node) is not present due to prior thermal activation. Spectroscopic properties, such as IR spectra, can also be calculated for the intermediates, as in Figure 6, for comparison with the experiment. Transition states can be calculated with saddle-point searching methods such as nudged elastic band (NEB),[100–102] dimer method[103,104] or Berny algorithm.[105]

This approach has allowed researchers to optimize MOF-based catalysts for a wide variety of energy and environmental applications, including hydrocarbon activation, toxic substance degradation, CO$_2$ reduction, and cross-coupling reactions. To fine-tune the catalytic performance of MOFs, DFT calculations have been utilized to investigate two crucial aspects in the design of MOF catalysts. The first aspect is the active site engineering, which typically involves tuning the coordinatively unsaturated metal sites and their coordination environment on the metal nodes. For example, previous studies have leveraged both the plane wave[106–113] and localized orbital[109,107,114–116] approaches to explore the optimal combination of the metal site and its surrounding ligands for enhanced C—H bond activation. The second aspect is tailoring the surrounding pore structure,[117] especially the pore surface functionality and size. Well-defined pore structures in MOFs can induce a confinement effect that restricts the movement and orientation of guest molecules within the confined space, altering their electronic and chemical environment, and thereby significantly enhancing catalytic activity and selectivity.

Compared with the plane wave approach, the localized orbital approach is more commonly used for engineering the active sites of MOF catalysts due to its higher computational efficiency, particularly in the search for transition state structures to calculate energy barriers in a catalytic process. However, the cluster

**ADVANCED
SCIENCE NEWS**

www.advancedsciencenews.com

**ADVANCED
FUNCTIONAL
MATERIALS**

www.afm-journal.de

approach does not include information on the surrounding pore structure and the resulting confinement effects, which can result in significant errors in the calculation of reactant and product binding energies, particularly in MOFs with smaller pores. For instance, in our recent study[118] on the hydrolysis of a nerve agent using Ti-MFU-4l, disregarding such confinement effects resulted in a 72 kJ mol^{-1} underestimation of the binding energy of the nerve agent on the reaction center, underscoring the plane wave approach's comparative advantage in estimating the confinement effect in MOFs.[118] Additionally, the localized orbital approach typically employs cluster models truncated from periodic models, which can result in ground spin states that are inconsistent with those in periodic models, particularly for MOFs with antiferromagnetic transition metal pairs.[119] In addition to these two approaches, the QM/MM (quantum mechanics/molecular mechanics) approach is an attractive strategy to model MOF catalysts. This approach treats the reaction center using quantum mechanics methods like DFT, while the remaining parts are treated using classical molecular mechanics methods, providing a reasonable compromise between accuracy and efficiency.[120,121] It is surprising that QM/MM is not used more frequently in modeling MOF catalytic processes.

There are several other factors that should be carefully considered when performing DFT calculations for MOF catalysts. First, the choice of exchange-correlation functional can significantly impact the accuracy of DFT calculations. Some widely used functionals include the GGA functionals like PBE, hybrid functionals like B3LYP, TPSSh, and PBE0, and the family of functionals developed by the group of Truhlar, such as M06-L, M06-2X, and MN15. It is a good practice to test multiple functionals using experimental or high-accuracy computational data as benchmarks to identify the most suitable functionals for specific applications. Second, the Hubbard +U correction[122] for transition metals is typically necessary for the plane wave approach to account for strong on-site electron-electron interactions not well-described by standard DFT exchange-correlation functionals.[123,124] The *U* value is typically determined by benchmarking against experimental measurements or employing higher-accuracy computational data to ensure an accurate representation of the properties of interest. Third, similar to the case of flexibility, the van der Waals interactions can play an important role in MOF catalysis systems, requiring accurate treatment using dispersion-corrected DFT methods described above. Finally, the effects of solvents or co-catalysts on performance in MOF catalysis systems need to be considered, which can be achieved using implicit solvation models like the polarizable continuum model (PCM), explicit solvent simulations, or a combination of the two.[125] It is always highly recommended to consult the relevant literature to determine the standard computational methods for the systems of interest.

3.5. Generation of Force Field Parameters

Beyond predicting reaction intermediates and transition states and analyzing the formation and breaking of chemical bonds, DFT calculations can also be employed to generate force fields for both molecules and frameworks, enhancing the understanding and prediction of adsorption behavior in complex systems

and facilitating classical adsorption simulations such as GCMC. QuickFF is a user-friendly method for generating force fields based on DFT calculations with a strong focus on MOFs.[126] QuickFF input data consists of ab-initio equilibrium geometries and a Hessian (it is used in vibrational frequency calculations) of smaller building units (linkers and metal nodes), and it uses simple mathematical expressions to represent the interatomic potential. The protocol was shown to be effective on a large set of organic molecules and MOFs, like MIL-53(Al) and MOF-5, generating accurate force fields for their periodic structures. This accuracy was confirmed based on the precision of molecule geometries, the unit cells of the MOF structures, and the vibrational frequencies. Notably, QuickFF is designed for parametrizing intra-molecular and intra-framework interactions, such as bonds, angles, and torsions, rather than long-range interactions like van der Waals or Coulomb. QuickFF has been implemented as an accessible Python code and is conveniently available online. QuickFF was recently updated to be able to use periodic ab-initio input data, and an extension to the energy expression was developed, including anharmonic bond and bend contributions together with the cross terms.[127] QuickFF was successfully used in a wide range of applications, including the analysis of phase transitions in COFs,[128] the mechanical stability of UiO-66,[129] contraction of CUK-1,[87] and thermal expansion in a large group of MOFs.[87]

Ab initio methods are commonly used in generating partial atomic charges for use in classical simulations. There are two general approaches for generating partial charges from DFT: electrostatic potential fitting and electron density partitioning. Here, we highlight two methods that are commonly applied in MOF studies: density-derived electrostatic and chemical (DDEC)[130–134] charges and repeating electrostatic potential extracted atomic (REPEAT) charges.[135] DDEC is a density partitioning method that allows for the determination of atomic partial charges, optimizes them to be chemically meaningful, and reproduces the electrostatic potential far from the high electron density region (far from the atoms, i.e., in the pores of MOFs). This method achieves this by optimizing atomic electron density distributions to resemble reference states and to be close to spherically symmetric around the atoms. DDEC accounts for different types of charge transfer, such as ionic bonding, covalent bonding, charge compensation, and dielectric screening, making it versatile and applicable to a wide range of materials. The REPEAT method is a simple and robust approach to derive charges in periodic systems based on fitting to the electrostatic potential generated by the electron density. It addresses the issue of the ill-defined offset in the electrostatic potential within periodic electronic structure calculations. This method can be applied to both molecular and periodic systems, providing physically reasonable and consistent charges. REPEAT charges show stability concerning variations in van der Waals radii and in electrostatic potential grid point density, and are particularly useful for simulating nanoporous materials like MOFs, offering a straightforward and automatable approach to deriving charges for periodic systems. In a benchmark analysis of various empirical and electron-density-based charges performed by Liu and Luan,[136] the authors used DDEC charges as a gold standard method emphasizing their transferability and consistency. Importantly, both DDEC and REPEAT methods are implemented in such a way that

2308130 (9 of 25)

**ADVANCED
SCIENCE NEWS**

www.advancedsciencenews.com

**ADVANCED
FUNCTIONAL
MATERIALS**

www.afm-journal.de

they can work with a variety of DFT software and both plane-wave and localized basis sets.

3.6. Machine Learning Tools to Facilitate DFT Calculations

As demonstrated above, DFT methods have garnered considerable interest due to their ability to analyze various phenomena in the MOF field, as well as aiding in the prediction of critical features for subsequent classical simulations (see below). This popularity is due to DFT's appealing balance between computational cost and accuracy in comparison to the more resource-demanding yet accurate correlated wavefunction theory. However, up until now, there has been no universally accurate density functional discovered, resulting in some degree of uncertainty in the quality of data produced by DFT. Duan et al. developed a density functional recommender approach[137] for selecting the best approximations to improve computational chemistry accuracy. The method uses neural networks together with transfer learning and was trained on a set of 300 transition metal complexes that are reasonably representative of MOF materials. The recommendation is provided based on the vertical spin splitting energy (energy between the high and low spin states of the complex) as a reference and was trained with data generated by (DLPNO)-CCSD(T) theory[138] that serves as a gold standard in modern computational chemistry. The recommender outperforms conventional methods and can be applied to various systems and computational methods. The recommender can be used alongside traditional high-throughput screening workflows without extra computational cost.

The same group developed an ML model that can predict ground-state spin states in metal complexes.[139] Remarkably, the model predicts the spin states only based on the structure. The authors used over 2000 experimentally characterized Fe(II)/Fe(III) complexes and employed a B3LYP-trained artificial neural network (ANN) to predict spin-state-dependent metal–ligand bond lengths and classify experimental ground-state spins based on agreement with the ANN predictions. This approach offers a promising alternative to the conventional energy-based spin-state assignment using electronic structure theory, with the low computational cost of a machine learning model. Jablonka et al. developed an ML model (oxiMACHINE) for predicting oxidation states in MOFs.[140,141] Their machine-learning model was trained on chemist-assigned oxidation states from the Cambridge Structural Database to automatically assign oxidation states to metal ions in MOFs. By considering only the immediate local environment around a metal center, the model is robust against experimental uncertainties such as incorrect protonation, unbound solvents, or changes in bond length. The method demonstrates good accuracy and was able to detect incorrect assignments in the Cambridge Structural Database. As MOFs garner increasing interest across various scientific fields, this method may prove especially beneficial for researchers working with these materials who may not possess a strong chemical intuition.

Furthermore, ML methods can facilitate geometry optimization tasks in high-throughput screening studies. Duan et al. introduced a dynamic classifier that monitors geometry optimization in real-time and terminates unproductive calculations.[142] This convolutional neural network model uses incremental information from DFT geometry optimization and generalizes well across various chemical spaces. By incorporating uncertainty quantification, the dynamic classifier can save more than half of the computational resources that would have been wasted on failed calculations, demonstrating its transferability and potential for catalyst design.

Illustrative of the potential of machine learning in the field of MOFs is the work by Moosavi et al., who employed a gradient-boosted ML model to predict heat capacity in MOFs.[143] Despite a training set of just over 230 MOF structures, the model demonstrated impressive accuracy with a root mean squared error below 3%. This study unveiled considerable variability in the heat capacity of MOFs, contradicting the common assumption of a constant value for most MOFs. Historically, researchers assumed a constant heat capacity for most MOFs when doing process level modeling due to a lack of data. However, this innovative model revealed that MOF heat capacities can vary between 0.4 and 1.2 J/g/K. This finding has significant implications for high-throughput screening studies, particularly when evaluating processes that involve heating or cooling of MOFs, where this contribution to the total heat must be considered, such as in adsorption cooling. Furthermore, this successful approach aligns with other achievements in the realm of ML applications for MOFs, such as predicting band gaps[144] or the bulk modulus.[145] Such accomplishments underscore the versatility and broad potential of ML in advancing MOF research (**Figure 8**).

4. Classical Methods for Modeling MOFs

For systems with a large number of atoms, DFT and other quantum mechanical methods can become infeasible due to the high computational costs involved. As an alternative, force-field-based simulation methods using models based on classical (versus quantum) mechanics and statistical mechanics are often employed to calculate thermodynamic and transport properties in MOFs, such as adsorption isotherms and the diffusion coefficients of guest molecules (**Figure 9**). In these methods, the energies and forces within the system are determined by classical potentials that describe interatomic interactions, rather than by solving the Kohn-Sham equations. In this section, we discuss two widely used simulation techniques: MD and grand canonical Monte Carlo (GCMC) simulations, with a focus on their applications to MOFs. We also explain some choices that are required to set up these simulations and review current advances in the field where machine learning is applied to assist and enhance the workflow of classical simulations.

4.1. Monte Carlo Simulations

Monte Carlo is a computational technique for calculating the thermodynamic properties of molecular or material systems by sampling configurations of the system based on their probability distribution under certain thermodynamic conditions. By averaging over the configurations, thermodynamic properties can be calculated, such as the number of adsorbate molecules in the system at equilibrium, heats of adsorption, virials, and heat capacities of the adsorbed phase. For MOF-related applications, gas
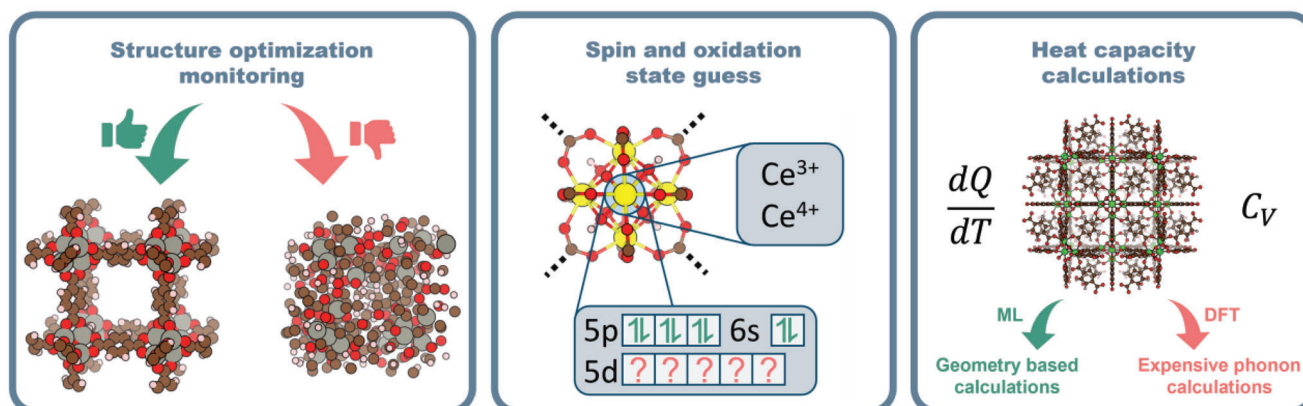
Figure 8. Examples of machine learning methods that can enhance DFT calculations: geometry optimization monitoring to discard meaningless structures, spin state and oxidation state recommender, and geometry-based heat capacity calculations.

adsorption is the central property of interest, and grand canonical Monte Carlo (GCMC)[146,147] or Gibbs ensemble Monte Carlo (GEMC)[148] simulations are naturally suited to serve the purpose. For instance, to simulate pure methane adsorption in a MOF,[46] the following steps are typically implemented in GCMC:

1) Set the chemical potential of methane (equivalently, the bulk phase pressure or fugacity), the number of unit cells of the MOF to be considered in the simulations (at least twice the interaction cutoff value to avoid self-interactions), and the system temperature. Generate an initial configuration of the system to start the simulation.

2) Pick an MC move randomly from a pool of possible moves such as insertion, deletion, translation, or rotation (note: the rotation move is specifically used for non-spherical molecules, which might have different orientations within the simulation box) of a molecule. The insertion or deletion moves ensure that the adsorbed phase reaches chemical equilibrium with the bulk phase, i.e., chemical potentials in both phases are equal. The translation and rotation moves ensure that the adsorbed phase reaches thermal equilibrium.

3) Either accept or reject the attempted MC move based on the change in the system energy and the Metropolis acceptance rule.[149,150]

4) Repeat steps 2 and 3 until the number of methane molecules (and the energy) in the system fluctuates around a constant value. The system is now equilibrated.

5) Continue steps 2 and 3 and calculate properties of interest by averaging over the configurations.

Figure 10 shows an example of three simulated isotherms of different types in MOFs.

In GCMC, the bulk phase (outside the MOF) is implicitly described by an equation of state (EOS) that relates the imposed chemical potential (or fugacity) with the bulk temperature and pressure (and composition if a mixture is simulated). In the simplest approach, the ideal gas EOS is applied, and the bulk phase fugacity equals the pressure. Alternatively, other EOS can be used, with the cubic Peng-Robinson EOS being one of the most common.[154] This EOS is parameterized using the critical parameters (temperature and pressure) and acentric factor of the fluid, which can be determined computationally for specific molecule models or taken from experimental data if there is good agreement between the model and experiment.

In comparison, GEMC uses two simulation boxes, both with periodic boundary conditions (as also used in the adsorbed phase box in GCMC): the first box models the adsorbed phase with
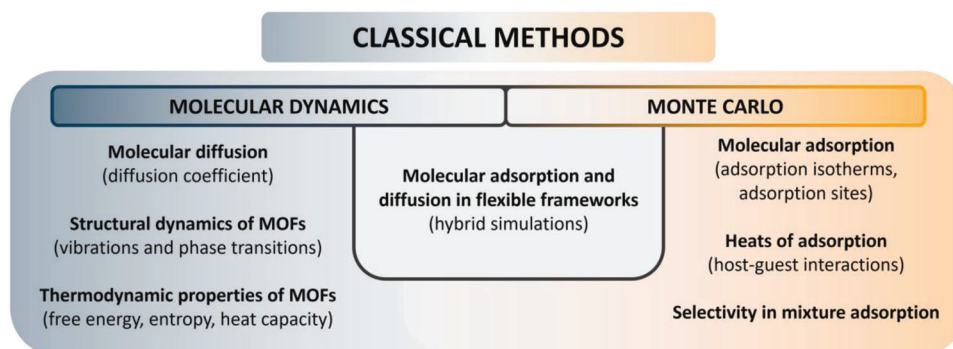

Figure 9. Schematic representation of problems that can be addressed by MD, MC, or both methods.
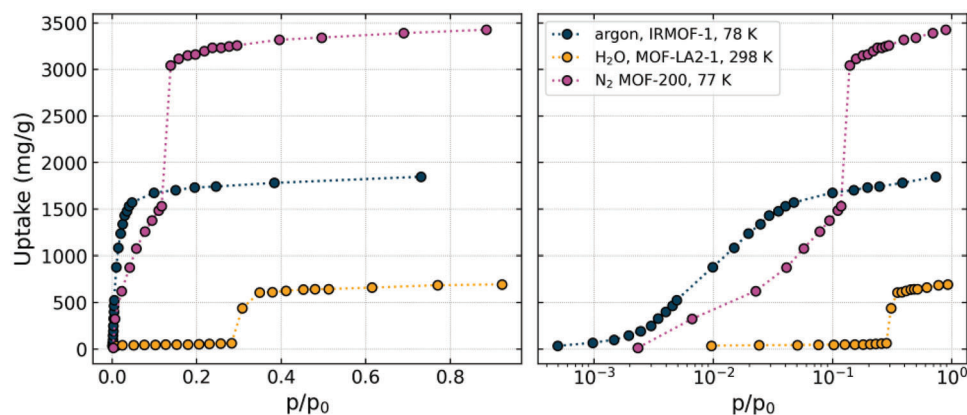
Figure 10. Simulated adsorption isotherms of different types: argon in IRMOF-1 at 78 K (type I), water in MOF-LA2-1 at 298 (type V), and nitrogen in MOF-200 at 77 K (type IV). Data taken from refs.[151–153] Isotherms are shown on the left with a linear pressure scale and on the right with a logarithmic pressure scale. Note the advantages of a logarithmic pressure scale for distinguishing differences in the low-pressure data.

the framework structure, and the second box explicitly models the bulk phase. The system temperature, pressure, and total number of molecules (sum of the number of molecules in both boxes) are set constant for the simulation. If the framework structure is assumed to be rigid, the volume of the adsorbed phase box is fixed, while the volume of the bulk phase box is allowed to expand or shrink to maintain the pre-defined pressure. During the simulation, in addition to the translation moves of molecules within each simulation box, molecules are also transferred between the two boxes. Such a transfer move is analogous to the insertion or deletion moves in the GCMC scheme. Again, MC moves are repeated until the system reaches equilibrium.

GCMC, predominantly utilized for gas adsorption, can be applied for simulations in open systems, allowing the exchange of molecules with an implicit bulk reservoir, thus speeding up the simulations. On the other hand, GEMC, originally tailored for phase equilibria simulation (vapor-liquid coexistence curve), demands an explicit simulation of both phases, either gas and liquid or bulk and adsorbed phases in adsorption simulations. For more technical details of MC simulations, we refer the readers to refs.[150,155,156]

Currently, a number of MC simulation packages are publicly available for modeling gas and liquid adsorption in MOFs.[155] In general, the software can be divided into two categories: CPU-based packages and GPU-based packages. CPU-based packages can use a serial or parallel implementation within a CPU framework. Several prominent options for CPU-based MC simulations are RASPA,[157] DL_MONTE,[158] Cassandra,[159] and Towhee.[160] GPU-based packages are designed to maximize the parallelization capability of GPU machines. This requires special implementation of conventional MC algorithms, such as distributing energy calculations to multiple cores on the GPU. GOMC[161] is an open-source MC simulation package that utilizes the parallelization power of GPU machines to accelerate multiple types of MC simulations. In addition to differences in their design framework, these MC packages also differ in their capabilities for performing certain statistical samplings and MC moves.

4.2. Molecular Dynamics Simulations

MD simulations predict the time evolution of the positions and velocities of individual atoms in a system by integrating Newton's equations of motion. Therefore, unlike the MC method, MD simulations can be used to extract dynamic information from the system. According to the ergodic hypothesis, over a long period of time, an MD simulation should lead to the same sampling of the phase space as an MC simulation at equilibrium. The dynamic nature makes MD simulations particularly useful for predicting transport properties, such as diffusion coefficients and relevant non-equilibrium phenomena where a pressure, temperature, or concentration gradient is present in the system.[156]

There are several open-source packages for conducting MD simulations. Some of the commonly used examples include LAMMPS,[162] NAMD,[163] GROMACS,[164] RASPA,[157] HOOMD-blue,[165] and DL_POLY.[158] The first three can take advantage of CPU parallelization with GPU acceleration. While NAMD is primarily applied in biological systems, LAMMPS and GROMACS are quite often used in MD simulations involving MOFs. Prior to an MD simulation of adsorbate molecules in a MOF, it is advisable to randomly distribute the molecules in the pore and perform an initial equilibration with a simple NVT-MC algorithm to avoid unphysically high forces in the system caused by overlap of the atoms. Such an initialization can be performed with any MC software such as RASPA. Alternatively, the energy of the guest molecules can be minimized via a geometry optimization algorithm. The simulated system should be equilibrated prior to the proper MD simulation (so-called production run). Equilibration is the process of allowing the system to reach a stable state before starting the production run, where data is collected for analysis. During equilibration, the system's properties, such as temperature, energy, pressure, or volume, should reach an equilibrium state where they fluctuate around their average values without any significant increase or decrease over a longer time scale. The number of equilibration steps needed to achieve this state can depend on factors such as the complexity of the system, the interactions between particles, and the initial conditions. Monitoring the system's properties (energy, temperature,

**ADVANCED
SCIENCE NEWS**

www.advancedsciencenews.com

**ADVANCED
FUNCTIONAL
MATERIALS**

www.afm-journal.de

pressure) during these equilibration steps allows one to determine when the system has reached a state of equilibrium. It is important to note that there is no fixed number of equilibration steps that applies universally to all systems. Determining the appropriate equilibration time often requires careful analysis and judgment based on the specific characteristics of the system being simulated. Following the equilibration procedure, the MD production run can be conducted for sampling the thermodynamic and transport properties of the system. The length of the simulation usually depends on the properties of interest. For instance, to calculate the self-diffusion coefficient of adsorbate molecules, the mean squared displacement needs to be proportional to time, and hence, the simulation should be continued until this requirement is satisfied. The time autocorrelation function of a specific variable can be another property that is monitored for adequate sampling. An autocorrelation function usually decreases from its initial value, which is one, to zero during a long enough MD simulation (relaxation time or correlation time). Therefore, for a proper sampling, the length of the MD simulation should be much longer than this relaxation time, and to reduce uncertainty, the sampling should be started after the relaxation time.[56] While it is possible to design MC moves to sample configurations of the solid framework, MD simulation is more natural and convenient to model the flexibility of the framework. Coupled with MC simulations, the hybrid MC/MD algorithm has been used to simulate gas adsorption in flexible frameworks.[166]

Here, we highlight several important applications of MD simulations to study phenomena in MOFs. These include simulations of molecular diffusion in complex pore landscapes and calculations of the thermal conductivity.

4.2.1. Diffusion

Various diffusion coefficients, including the self-diffusion coefficient (also known as the self-diffusivity), are among the important physical parameters that can be calculated using MD simulations. To calculate the self-diffusion coefficient of adsorbate molecules in MOFs, the mean squared displacement (MSD) of each molecule is tracked during the MD simulation, and the self-diffusivity can be calculated from the Einstein equation:[150,156]

$$D_s = \lim_{t \to \infty} \frac{1}{2dt} \frac{1}{N} \sum_{l=1}^{N} \left[r_l(t) - r_l(0) \right]^2 \tag{2}$$

where d is the dimensionality of the system (1,2 or 3), t is time, N is the number of molecules, and r_l is the position vector of the l-th molecule. While the equation above includes an average over the different molecules in the system, a good practice is to further increase the statistics and include an average over all possible time intervals τ:

$$\text{MSD}_{av}(\tau) = \frac{1}{N} \sum_{l=1}^{N} \sum_{\tau=\Delta t}^{n\Delta t} \left(\frac{1}{n - \frac{\tau}{\Delta t} + 1} \sum_{t=0}^{n\Delta t - \tau} \left[r_l(t+\tau) - r_l(t) \right]^2 \right) \tag{3}$$

$$D_s = \lim_{\tau \to \infty} \frac{1}{2d\tau} \text{MSD}_{av}(\tau) \tag{4}$$

In this equation, n represents the number of timesteps in the simulation, effectively defining the simulation's length. The first summation accounts for the number of molecules in the system, the second for the average over multiple time intervals τ, and the third ensures consideration of all possible time origins for the MSD calculations for a given τ (see **Figure 11** for details). The shortest possible time interval is the same as the time step Δt chosen for the simulations; however, for practical considerations, often a slightly larger interval is selected as the shortest one. The largest interval is the total simulation time. $n - \frac{\tau}{\Delta t} + 1$ is the total number of summation terms of a given time interval used in averaging over multiple time origins. Note that D_s should be calculated for the range in which the MSD is proportional to the time interval.[167] Complete details for calculating the self-diffusivity of adsorbate molecules are provided by Sharp et al.[168] For a simulation of a bulk fluid, the number of degrees of freedom (DOF) is typically given by 3N-3, where 3 degrees are subtracted to account for the conservation of the momentum of the center of mass of the system. However, when performing molecular dynamics (MD) simulations with an external field (such as a rigid framework or implementing a temperature or pressure control algorithm), this conservation is no longer valid, and the number of DOF becomes 3N. This distinction becomes important when considering temperature calculations in MD simulations, as it can impact the accuracy in calculating certain properties, like diffusion coefficients, particularly in systems with a low number of particles (less — than 50). Xu et al.[169] provide examples that specifically tackle this concern, offering solutions for some of the commonly used MD codes.

Several studies have been performed to determine the self-diffusivities of diverse adsorbate molecules in MOFs.[168,170] For instance, Bukowski and Snurr studied the effect of topology in 38 MOFs on the diffusion of alkanes.[171] The most interesting aspect of their work is the clear demonstration that MOF topology — the arrangement and interconnectivity of pores—significantly affects the diffusivity of guest molecules such as propane and isobutane, with their self-diffusion coefficients spanning more than two orders of magnitude across different Zr_6 MOF topologies. This reveals that slight changes in the internal structure of MOFs can dramatically alter their physical characteristics, demonstrating the tunability of MOFs. Moreover, the observation that the node connectivity influences the propane diffusivities more than the MOF pore limiting diameter, especially at low loading, illustrates how complex these materials can be. This complexity offers a wide spectrum of potential applications, but also hints at the challenges faced in designing and optimizing MOFs for specific uses.

Experimental screening of MOFs to gain physical and chemical insights into the connection between MOF structure and adsorbate diffusion is challenging, but with increasing computer speed, it is now possible to use simulation to provide such insights. For example, the diffusivities of the chemical warfare agent (CWA) simulant dimethyl methyl phosphonate (DMMP) were calculated for 776 hypothetical MOFs with Zr nodes and different pore sizes.[172] The data were analyzed using machine learning, which revealed that the node-node minimum distance, gravimetric surface area, volume fraction of nodes, and MOF density were the most important parameters for predicting the self-diffusivity of DMMP in these MOFs. It was found that the same model could be used to predict the diffusivity of sarin in the same structures.
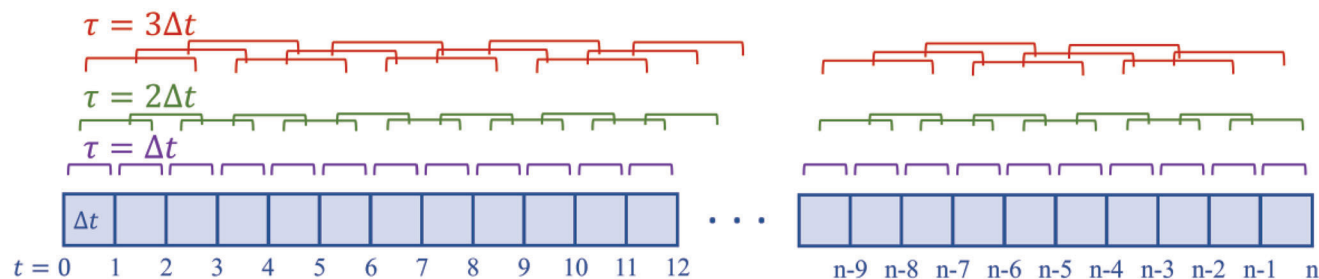
**ADVANCED
SCIENCE NEWS**

www.advancedsciencenews.com

**ADVANCED
FUNCTIONAL
MATERIALS**

www.afm-journal.de

Figure 11. The time interval (τ) is depicted over stored MD configurations. For each $\tau = i \cdot \Delta t$ ($i = 1$ to n), squared displacements are calculated and averaged to calculate the MSD at that $i \cdot \tau$.

4.2.2. Thermal Conductivity

The thermal conductivity (κ) is another physical property that can be calculated for MOFs using equilibrium NVE MD simulations by analyzing an autocorrelation function:

$$\kappa = \frac{V}{k_B T^2} \int_0^\infty \langle \mathbf{J}(t) \cdot \mathbf{J}(t+\tau) \rangle d\tau \tag{5}$$

where V is the volume of the system, k_B is the Boltzmann constant, T is temperature, $\mathbf{J}$ is the heat flux vector, and the angular brackets denote an ensemble average. $\mathbf{J}$ can be calculated as:

$$\mathbf{J}(t) = \frac{d}{dt} \sum_i r_i E_i = \sum_i \left(v_i E_i + r_i \frac{dE_i}{dt} \right) \tag{6}$$

where r_i, E_i, v_i are the position vector, energy, and velocity of the i-th atom, respectively.[150,173–175] This calculation requires that MOF framework flexibility is taken into account. As an example, the thermal conductivity of IRMOF-1 has been studied using MD simulations between 200 and 400 K.[176] MD simulations were performed on variously sized systems comprising 1, 8, and 27 unit cells. The findings pointed to a specious correlation between thermal conductivity and simulation system size. This underscores the need for a sufficiently large system size to minimize potential errors associated with smaller systems. The size and shape of the pores of a MOF, together with the presence of adsorbed molecules, can also influence the thermal conductivity. In a study that concentrated on idealized MOFs, it was found that the thermal conductivity of MOFs with small pores decreased in the presence of the adsorbed gas molecules.[177] However, the presence of adsorbed gas molecules did not affect the thermal conductivity of MOFs with large pores.

High-throughput calculations were performed by Islamov et al. to calculate the thermal conductivities of 10 194 hypothetical MOFs.[178] The results showed that MOFs with four-connected metal nodes, small pores, and high density have higher thermal conductivities and that MOFs with extremely large pores are characterized by ultra-low thermal conductivities. In addition, the influence of porous crystal flexibility (pore expansion, as a model for MOF breathing transition) on thermal conductivity has been studied in the presence of adsorbed gas.[179] The thermal conductivity was calculated for a range of structures from the completely closed to fully open form. The study concluded that thermal conductivity shifts only in accordance with the direction of crystal expansion, irrespective of adsorbed gas presence. Interestingly,

this change in thermal conductivity is less noticeable when guest molecules are present.

4.3. Models for Classical Molecular Simulations

Best practices, in general, for performing classical MD and MC simulations have been extensively discussed in other places.[150,180] In the field of MOFs, two components are particularly important for an accurate and high-quality simulation: the MOF structure and the force field that describes the guest-host, guest-guest, and intra-host interactions. In this subsection, we discuss best practices for the preparation of MOF structures and the selection of suitable force fields.

4.3.1. Crystal Structures

One of the most significant challenges in classical simulations of MOFs and the phenomena occurring within their pores is the accurate representation of their structure. The MOF structure for molecular simulations can be either obtained from single-crystal X-ray diffraction (XRD) experiments or constructed in silico. If an experimentally resolved crystal structure is available, this is usually the best approach. Since MOFs are crystalline materials, this sounds straightforward, but there are several challenges in practice. First, hydrogen atom positions cannot be obtained directly from XRD, and hydrogen atoms are usually added using crystallographic software. Placing the missing hydrogen atoms on an aromatic ring is straightforward, but automated software may struggle to make the correct assignment of whether an oxygen atom is part of a hydroxyl group or a bound water molecule. For example, the proton topology on the 8-connected Zr_6O_8 nodes of MOFs like NU-1000 cannot be determined from diffraction experiments. In this case, DFT calculations were used to identify the most stable configuration,[181] and this configuration has subsequently been used in molecular simulations. Another challenge is that crystal structures may contain partial occupancies and other forms of disorder, which must be "cleaned" before the structure can be used for simulations. The presence of solvent molecules within the crystal structure of MOFs presents a significant challenge. During adsorption experiments, these molecules may be eliminated in the activation process. Ideally, an adsorption simulation should mirror these experimental conditions accurately, which implies the removal of these solvent molecules. However, confirming that each solvent molecule has

**ADVANCED
SCIENCE NEWS**

www.advancedsciencenews.com

**ADVANCED
FUNCTIONAL
MATERIALS**

www.afm-journal.de

Table 1. Summary of representative large MOF databases.

Database	Year	Structure type	Number of structures	Features
hMOF-Wilmer[50]	2012	Hypothetical	137953	Hypothetical structures for high-throughput materials discovery
CoRE MOF 2014[18]	2014	Experimental	5109	Curated and cleaned experimental structures ready for molecular simulations
ToBaCCo[184]	2017	Hypothetical	13511	MOF structures with enhanced diversity in topology and pore size
CSD MOF subset[189]	2017	Experimental	69666	Reported to be the most complete collection of experimental MOF structures, actively updated
MTV-MOFs[190]	2017	Hypothetical	≈10000	Multivariate MOFs with mixed linkers and functional groups
BW-DB[191]	2019	Hypothetical	325000	Database for accelerating the discovery and optimization of materials for carbon capture
CoRE MOF 2019[17]	2019	Experimental	14845	Update of 2014 CoRE MOF database
hMOF-Lan[192]	2019	Hypothetical	303991	MOF structures with diverse channel types and enhanced topology distribution
hMOF-Majumdar[193]	2021	Hypothetical	≈20000	MOF structures with enhanced structure diversity
QMOF[144]	2021	Hybrid	14000	DFT-optimized MOF structures
hMOF-Nandy[194]	2023	Hypothetical	≈50000	MOF structures with enhanced thermal and activation stability

indeed been eliminated during the experiments can be complex. Furthermore, extracting these solvent molecules can trigger pore collapse in MOFs, especially those with large mesopores. Consequently, relying on "cleaned" structures in simulations might not always accurately reflect the real activated material.

Databases of MOF structures from experiments have been constructed in the past few years to facilitate molecular simulations and high-throughput materials discoveries, as listed in **Table 1**. Experimental MOF structures curated in these databases usually undergo semi-automated processes. It is important to note, however, that while these processes aim to clean the disorder and remove unwanted solvent molecules, their effectiveness is not absolute. There may be instances where mis-bonded or isolated atoms remain. As an example, Chen and Manz[182] found it necessary to propose extra procedures to clean structures from the 2019 CoRE MOF database[17] with such issues. Hence, users of these databases should be aware of these limitations.

Alternatively, MOF structures can be constructed on the computer from their constituent nodes and linkers using available construction algorithms, such as AuToGraFS,[183] ToBaCCo,[184,185] TOBASCCO,[186] and PORMAKE.[187] These construction algorithms typically map the building blocks (nodes and linkers) onto a topological blueprint, and building blocks are connected through pre-defined connection points. The constructed structures are usually optimized using either a classical force field, such as the Universal Force Field (UFF)[188] or DFT before they are fed into the simulation workflow. Due to the unique combinatorial nature of MOF structures, the computational construction method opens the door to the generation of an infinite number of hypothetical MOF structures. This paradigm naturally fits in with a high-throughput screening workflow and has accelerated materials discovery at an unprecedented speed.

4.3.2. Classical Force Fields for Adsorption Simulations

Most classical force fields are composed of a set of equations describing interatomic interactions such as bond stretching, bond angle bending, dihedral angles, and non-bonded interactions. The force field also includes the parameters in these equations. The non-bonded interactions include attractive dispersive (van der Waals) and repulsive interactions (often modeled with a Lennard-Jones potential between all pairs of non-bonded atoms) and long-range Coulombic interactions (often modeled by placing point charges on the atoms). For more details and the inner workings of force fields in molecular simulations, we refer readers to refs.[56,195]

One of the difficulties in developing a force field for MOF simulations is the enormous chemical diversity of these materials and the wide range of potential applications. Ideally, a good force field is both transferable and accurate. There are two main approaches for developing a force field. In the first, the parameters are fitted against DFT or other quantum mechanical calculations such as MP2 or CCSD. In this approach, the parametrization process involves determining the parameters of the force field that minimize the difference between the energies and forces predicted by the force field and those calculated using quantum mechanical methods. Often, the fit is performed using a set of molecules and configurations that is representative of the system of interest. This process can be complex and time-consuming, as it involves iterative optimization of many parameters. Another aspect to consider is that while this approach can lead to high accuracy for the systems that the force field was trained on, its transferability—that is, its ability to accurately predict the properties of systems that are not in the fitting set—is not always guaranteed. Ensuring transferability is a major challenge in force field development, requiring careful design of the functional form of the force field and the selection of the training set. In the second approach, the force field is fitted so that the results match some reference experimental data such as adsorption isotherms and heats of adsorption. A challenge for this approach is that there may be differences in reported experimental data for a given system due to different materials synthesis and activation strategies applied. Another issue is that most simulations of adsorption in MOFs to date have assumed a rigid framework structure. If the MOF exhibits significant flexibility and the MOF is assumed rigid in the

**ADVANCED
SCIENCE NEWS**

www.advancedsciencenews.com

**ADVANCED
FUNCTIONAL
MATERIALS**

www.afm-journal.de

simulations, then fitting the force field to match experiment will likely lead to an unreliable force field.

In practice, force fields in the MOF field are often not assembled "from scratch" but by starting with existing force fields. The most common approach is to employ a "generic" force field for the adsorbent (i.e., a force field that was not developed specifically for MOFs) alongside a force field for the adsorbate taken from previous work on bulk fluids. Simulations of vapor-liquid equilibrium, including coexistence curves and saturation pressures, serve as a rigorous assessment of the accuracy of fluid force fields. Therefore, we strongly recommend the use of force fields that have been tested to predict these quantities in good agreement with experiment. An example of such a force field is the Transferable Potentials for Phase Equilibria (TraPPE).[196] Often, the UFF[188] or a combination of Dreiding[197] and UFF is used for the framework. This could include equations and parameters for treating MOF flexibility or simply taking the Lennard-Jones parameters from these force fields and using them for the MOF atoms, which are held fixed at their crystallographic coordinates. Vandenbrande et al.[198] performed a benchmark analysis of the accuracy of predicting methane uptake in Zr MOFs with both generic force fields (UFF and a combination of UFF and Dreiding). They compared them to three more sophisticated force fields: MM3-MBIS,[199] SAPTFF,[200,201] and MEDFF,[202] the latter two of which are purely ab initio derived. They concluded that at moderate pressure, the generic force fields are reasonable and can be used to predict quantities such as the working capacity close to saturation pressure. Recently, an online adsorption database, MOFX-DB,[203] was constructed to facilitate the use and reproducibility of simulated gas adsorption data in nanoporous materials. MOFX-DB contains simulated adsorption isotherm data for more than 160 000 MOF and zeolite structures. All necessary simulation input files are also available in the database to enhance the reproducibility of data. The simulated data in MOFX-DB can help validate force fields parameters against experimental data in a holistic manner.

Partial charges on the atoms can have a strong influence on the predicted properties and behavior of the system. For the adsorbate atoms, the partial charges are usually taken from the force field used for the adsorbate (e.g., TraPPE). However, partial charges for framework atoms are usually calculated for each MOF as needed. As described in Section 3.5, framework charges are often obtained from DFT. There are, however, a wide range of empirical methods that can be used to calculate these charges much faster than DFT. One of the first empirical methods developed for determining partial charges was the charge equilibration (QEq) method.[204] It is designed to compute partial charges of atoms within a molecule, utilizing the molecular geometry and three atomic properties. These properties are the ionization potential, which signifies the energy required to remove the outermost valence electron, the electron affinity, indicating the energy variation associated with the addition of an extra electron, and the atomic radius. These parameters can either be derived from experimental findings or calculated through ab initio methods. Many developments of this method were reported in the literature, including extended (EQEq), which improved the accuracy of metal cation charges (with the intention to apply in MOFs),[205] and the MOF electrostatic-potential-optimized charge (MEPO-QEq) scheme, in which the parame-

ters (electronegativity and chemical hardness) were trained based on DFT calculations for a group of 543 MOFs.[206] Ongari et al. performed a benchmark analysis of Qeq and its derivatives, revealing specific issues related to atom types and input parameters in the assessment of 2338 MOFs.[207] Their study highlighted that Qeq methods have not shown significant improvement in accuracy over time. Since these methods are not computationally expensive, they can be used in high-throughput screening studies, although it is suggested to re-test the top-performing candidates with simulations based on partial charges from DFT.

In classical simulations of adsorption in MOFs, another important factor that can significantly influence the outcomes, is the tail correction. It is a mathematical formula applied to compensate for the truncation of long-range interactions in the system. The tail correction and the chosen cutoff radius – the limit beyond which interparticle interactions are neglected—can substantially affect simulation results. If a force field has been designed with specific cutoff radii and with the consideration of the tail corrections, these parameters should always be used to ensure the reliability of the results. Jablonka et al. demonstrated that the homogeneous tail corrections tend to yield results that are less affected by the cutoff radius, making them a preferable option.[208] This conclusion is consistent across a wide range of structures tested, including zeolites, metal-organic frameworks, and covalent organic frameworks (see **Figure 12** for details). Furthermore, since there is no universal cutoff value for the potential, the study recommends the application of tail corrections in modeling gas adsorption in microporous materials. This is proposed to facilitate a more consistent and reliable comparison of results derived from different simulation studies. Note, however, that there are certain force fields that were optimized without tail corrections, and for these models, the application of tail corrections may not be advisable.[209] Regardless of the choice, all details of the simulation—including the cutoff distance and whether or not tail corrections were applied—should be reported in publications reporting simulation results to ensure reproducibility.

The lack of universal intramolecular force fields for MOFs is the main challenge for considering flexible frameworks in MD simulations. Nevertheless, there are some studies that concentrated on the effect of framework flexibility on the diffusion of adsorbate molecules by implementing currently available force fields such as UFF4MOF,[210] AMBER,[211] and CVFF[212] or using ab initio calculations to develop force field parameters for specific MOF structures, as discussed in Section 3.5. The modified CVFF force field was used for a flexible UiO-66(Zr) MOF to calculate the D_s of CH_4 in CO_2/CH_4 mixtures at different CO_2 loadings. Although D_s obtained by quasi-elastic neutron scattering (QENS) was higher than the calculated D_s by a factor of 2.5, both experimental and simulation trends were similar at a low loading of CO_2.[213] The diffusion, adsorption, and separation of various molecules in a family of ZIFs have been studied using equilibrium MD simulations and transition state theory (TST) methods. Since ZIF frameworks, such as ZIF-8, have relatively small pores, including framework flexibility in the simulations is beneficial for obtaining accurate diffusion coefficients. Certain force fields established through DFT calculations for this set of structures demonstrated good accuracy in predicting
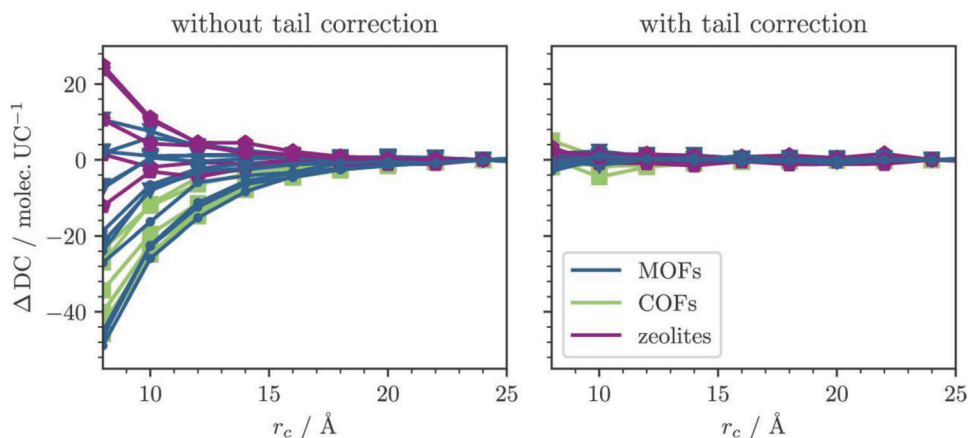
**ADVANCED
SCIENCE NEWS**

www.advancedsciencenews.com

**ADVANCED
FUNCTIONAL
MATERIALS**

www.afm-journal.de

Figure 12. Impact of the application of the tail correction on the absolute error in deliverable capacities of methane in porous materials ($\Delta DC = DC(r_c) - DC(r_c = 24\ \text{Å})$). Reproduced with permission.[208] Copyright 2022, American Chemical Society. Further permission requests related to this figure should be directed to the ACS.

self-diffusivities and corrected diffusivities, aligning closely with experimental findings.[214–221] In each of these studies, some interesting physical insights about the relation between the diffusivities and framework flexibility were described. It was shown that the substitution of metal cation in the ZIF-8 framework, creating ZIF-67 (Zn to Co substitution), led to a notable enhancement in ethylene/ethane separation efficiency. The metal variation appeared to govern the aperture size and stiffness, as confirmed by simulations.[73,221] In addition, simulation results indicated that implementing different force field parameters led to order of magnitude differences in diffusivities.[214–215,221] While these simulations offer valuable insights into the behavior of flexible MOFs, the significant disparities in diffusivities depending on the choice of force field parameters underscore that current simulation methods may not fully capture the complex interplay of framework flexibility and diffusive behavior, necessitating further refinement and validation of these models. Yang and Sholl studied the importance of framework flexibility on the diffusivities of 12 different adsorbates with different sizes, shapes, polarities, and flexibilities in 17 different MOFs.[222] UFF4MOF was used for flexible and rigid frameworks. In many examples, simulations with rigid frameworks underestimated the diffusivity of molecules in MOFs with small pores. The results demonstrated that the correlation between the flexibility of the framework and diffusivity depends on the size of the pore and the adsorbate. When the size difference between windows and adsorbate is greater than 4 Å, the flexibility of the framework has a small influence on the diffusion. However, the effects of diverse functional groups, metals, and linkers on the mobility of various flexible ZIF MOFs and the diffusivity of adsorbate molecules are complex. To address this issue, ML methods were used on 14 different adsorbates in 72 existing and hypothetical flexible ZIFs with SOD topology.[223] The trained ML approach uses simple, readily available input information to train predictive models that bypass extensive computational steps and directly estimate the diffusivity of penetrants in newly functionalized ZIF-8 variants.

The breathing behavior of some MOFs has been studied using MD simulations. For example, the flexible MIL-47(V^{IV})

was investigated using the CVFF force field. MD simulations were conducted at 300 K and at a variety of external hydrostatic pressures up to 350 MPa. The simulation results demonstrated the phase transition in MIL-47 under diverse pressure range is in good agreement with X-ray powder diffraction results.[224] Framework breathing was also studied in the presence of adsorbates at different loadings.[225,226] Using NVT and NPT MD simulations, along with GCMC simulations, the flexible IRMOF-74-V was studied with Ar as an adsorbate, using the CVFF force field. The results successfully predicted the deformation of the MOF, aligning with experimental adsorption and X-ray diffraction data.[225] In the second report, MD simulations were utilized to explore the breathing behavior of the flexible MIL-53(Cr) across a range of CO_2 uptakes. The predicted unit cell parameters for MIL-53(Cr) exhibited excellent agreement with the results from in situ X-ray diffraction experiments.[226]

In addition, it is worth mentioning a distinctive and transferable forcefield, VMOF, that was developed specifically for metal-organic frameworks to accurately determine a broad range of properties related to lattice dynamics, such as phonon spectra, thermodynamic and mechanical properties, free energies, heat capacities, and bulk moduli.[227] This approach, tested on MOFs such as IRMOF-1, UiO-66, and MOF-74, can help facilitate high-throughput computational screening of vibrational properties across a diverse range of MOFs.

4.4. Machine Learning Methods to Facilitate Classical Simulations

Recent advances in machine learning are providing new routes to solving some of the most challenging problems in classical molecular simulations. In this subsection, we discuss two recent notable ML developments for molecular simulations of MOFs, i.e., ML force fields and using ML to obtain partial charges. These developments help tackle the traditional tradeoff between computational expense and accuracy of the simulation. Current challenges and future directions are also discussed.
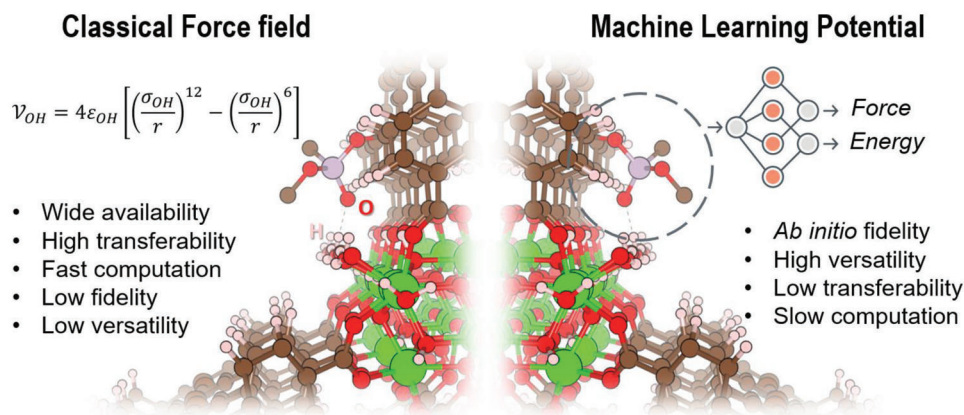
ADVANCED
SCIENCE NEWS

www.advancedsciencenews.com

ADVANCED
FUNCTIONAL
MATERIALS

www.afm-journal.de

Figure 13. Comparison of classical force fields and machine learning potentials.

4.4.1. Machine Learning Force Fields

The purpose of a force field is to accurately reproduce the potential energy surface of a system (**Figure 13**). As described above, classical force fields can be obtained by fitting the potential energy surface obtained from ab initio calculations to a certain functional form. The functional form can be physically rigorous, such as the Coulombic potential, or it can be semi-empirical, such as the 12-6 Lennard Jones potential, where the $(1/r)^6$ term was derived from London dispersion forces, but the $(1/r)^{12}$ term was chosen for convenience to approximate Pauli repulsion. Restriction to a pre-defined functional form may limit its applicability to describe certain effects, such as possible quantum diffraction effects, many-body interactions, and reactions, where special treatments are needed.

With the capability to approximate any functional form, ML models, such as neural networks[228] and Gaussian process regression,[229] have been developed to predict the potential energy surface of a system with the accuracy of DFT but much faster. Figure 13 shows a comparison between classical force fields and ML potentials. For a standard ML potential model, the general idea is that by training the ML model with data points from quantum mechanical calculations, the ML model is able to predict the system energy and atomic forces with ab initio level accuracy, based on the local environment of each atom as input. ML potentials inherently account for any quantum effects, many-body effects, and possible chemical reactions that are encoded in the ab initio training data.

ML potentials have become prevalent in the past few years largely due to the availability of user-friendly software and tools[228,229] and increased computational power to generate a large amount of reliable ab initio training data. ML potentials for MOF systems have appeared very recently. To accurately model molecular diffusion in flexible MOFs, Achar et al.[230] developed a hybrid simulation scheme by applying different modeling strategies to guest-guest, guest-host, and intra-host interactions. They developed a ML potential to describe the intra-host interactions for UiO-66, while for guest-guest and guest-host interactions, a conventional LJ potential was retained to reduce the computational expense. They found that this hybrid modeling scheme can reliably account for the motion and flexibility of the MOF struc-

ture in response to the presence of adsorbate molecules such as Xe and Ne. In their work, they applied a two-phase training scheme, with the first stage focused on training the model to accurately predict the energy-volume response, and with the second stage focused on generating structures at elevated temperatures to explore more of the configurational space of the materials. Indeed, how to efficiently generate training data for ML potential model development is still an open question. Vandenhaute et al.[231] built an incremental learning workflow to train a ML potential for framework materials. The workflow implements an on-the-fly training strategy for the ML potential, with training data iteratively collected from parallelized quantum mechanical and metadynamics simulations. The metadynamics component in the workflow helps to explore the free energy landscape and learn the structural phase space of flexible MOFs in a more effective manner. With only a few hundred single-point DFT evaluations per material, an accurate and transferable ML potential based on an equivariant neural network was obtained. Similarly, guest-host interaction energies can also be predicted by ML potential models. Yang et al.[232] developed a deep ML model to learn the potential energy surface of guest molecules near a framework structure. Their model takes the transformed distance between adsorbate molecules and the framework as input features and predicts the guest-host energies with DFT level accuracy. They validated their ML potential by comparing computed Henry's coefficients using the ML potential and a reference force field fitted against the DFT data in their previous work.[233]

The development of ML potentials for MOF systems is still in its infancy. Further research in this area is necessary to solve several outstanding challenges. For example, compared to classical force fields where the functional forms are physically meaningful, an ML potential works as a black box. Building an interpretable ML potential is still an ongoing goal in the field. In addition, most of the current ML potentials use each atoms' local environment (within a certain cut-off) as input features. A full understanding of how the long-range interactions are accounted for and what role they play in controlling the system properties is still lacking.[234,235] Regarding the transferability of ML potential models across different material types, several research groups have attempted to develop so-called foundational or universal ML potentials, such as ANI-1,[236] MEGNet,[237] M3GNet,[238] and

ADVANCED
SCIENCE NEWS

www.advancedsciencenews.com

ADVANCED
FUNCTIONAL
MATERIALS

www.afm-journal.de

CHGNet.[239] Yu et al.[240] applied the MEGNet model to predict the mechanical properties of defective MOFs. However, whether these universal models can be reliably applied to MOF materials in general is still unclear. Future efforts could be focused on systematic benchmarking of existing universal ML potentials against classical force fields (e.g., UFF4MOF[241]), reference ab initio data, and experimental results.[242] It would also be beneficial to develop a new universal ML potential model for MOF materials or fine-tune existing models using MOF training data. Finally, we note that molecular simulations using ML potentials are generally slower than those using classical force fields. However, they are well suited for GPUs, and simulation codes that use GPUs may be very helpful in expanding the usage of ML force fields. These efforts should allow researchers to simulate systems at larger spatial and time scales at DFT-level accuracy.

4.4.2. Partial Charges from Machine Learning

Partial charges, as discussed above, can be calculated through two main approaches: DFT calculations and empirical methods. DFT, while highly accurate, tends to be time-consuming. Empirical methods, on the other hand, are faster, but they are sometimes less accurate. ML presents an elegant solution that has the potential to predict partial charges for MOFs with DFT-level accuracy, yet with significantly reduced computation time. Zou et al. developed the multilayer connectivity-based atom contribution (m-CBAC) method,[243] which assigns charges based on averaging the DDEC charges for atom types with the same connectivity pattern. It is based on the CBAC method,[244] but it is trained on a significantly larger set of MOFs (2700 versus 43) and uses three layers of connectivity instead of one (0—central atom, 1—central atom and nearest neighbors, 2—central atom, nearest neighbors, and 2nd nearest neighbors). When assigning a charge to a target MOF atom, the system first searches for the 2nd nearest neighbor connectivity pattern, which provides the most accurate charge assignment. If this is unavailable, it moves to the 1st and then the 0th layer, which is less accurate but broadly applicable. The method was also tested for accuracy by predicting CO_2 Henry's constants for MOFs not included in the training set and demonstrated better accuracy compared to the EQeq method. Charges assigned using the m-CBAC approach were discovered to closely mirror DDEC charges, as indicated by a Pearson correlation coefficient of 0.99. The computational resources needed for this approach are comparable to those of the EQeq method, but substantially lower than those required for DFT calculations. Raza et al. created and trained a message passing neural network (MPNN) to learn representations of local bonding environments within MOFs and to predict the partial charges on the atoms of a MOF under a charge neutral constraint.[245] The crystal structure of the MOF, represented as an undirected graph with node features encoding the chemical elements, is directly inputted into the MPNN. The MPNN builds features of the local bonding environments by passing information between bonded atoms. It was trained and evaluated using 2266 MOFs with DDEC-assigned charges. The MPNN predicts the partial charges with a mean absolute deviation from DDEC charges on the test set of 0.025, while requiring significantly less computational time than performing electronic structure calculations to derive the charges.

Kancharlapalli et al. proposed another ML method, referred to as PACMOF, for predicting partial charges trained using a random forest algorithm based on 950 MOFs with DDEC charges.[246] In addition to local bond environment features, they also considered elemental properties such as ionization potential and electronegativity, which ensured good accuracy (MAD = 0.026, correlation coefficient = 0.99). The model was validated using a different set of MOFs comparing not only charges but also the simulated adsorption isotherms.

Partial charges, while not an experimental observable, play an important role in classical force field descriptions of the energetic interactions in MOFs. Therefore, comparing adsorption isotherms generated using ML-generated partial charges forms an essential part of the evaluation and refinement of different methodologies for determining partial charges. CRAFTED is a database of simulated isotherms that explores the impact of different force fields and charge methods (including PACMOF and MPNN) on CO_2 and N_2 adsorption in MOFs.[247] Burner et al. reported REPEAT charges for about 280000 experimental and hypothetical MOFs,[248] and this database also provides extensive and diverse training and testing data for building new ML models for partial charge prediction.

5. Conclusions

This review has provided an overview of the essential role of computational research in understanding MOF properties and phenomena by focusing on three widely used molecular modeling methods: density functional theory, Monte Carlo simulations, and molecular dynamics simulations. We explored the properties that can be calculated from DFT, examining the distinctions between periodic and cluster methodologies and to which problems they can be applied. We emphasized the importance of DFT as a standard method for conducting the initial steps of simulations involving MOFs, such as accurate geometry optimization or generating partial charges, for subsequent studies employing classical methods. Moreover, we discussed the problem of framework flexibility and demonstrated how DFT can aid in predicting structural transformations and thermodynamic properties using energy-volume relations and phonon analysis. We also explored the potential of cluster models of metal nodes in MOFs for understanding the nature of host-guest interactions and catalytic reactions. Additionally, we discussed accessible and efficient methods for generating ab-initio derived force fields, which hold significant promise for applications in classical simulations. In conclusion, DFT can be appreciated from two distinct perspectives: as a valuable tool for conducting an initial analysis of MOF structures prior to subsequent simulations and as a method capable of elucidating phenomena not encompassed by classical approaches. This dual functionality highlights the versatility and significance of DFT in the field of MOF research and its vital role in driving progress and deepening our understanding of these remarkable materials.

For classical simulations, we discussed the importance of force field selection for simulations of adsorption and diffusion. We highlighted the available databases of materials suitable for high-throughput screening and addressed potential challenges that may arise. The classical methods of MD and MC are complementary. MD is particularly useful for investigating dynamic

processes such as diffusion, conformational changes, and the response of materials to external forces. For instance, MD simulations can predict diffusivities of various adsorbates within the MOF, shed light on diffusion mechanisms and pathways, and monitor changes in MOF or adsorbate structures over time. Importantly, MD simulations can account for the flexibility of MOFs, revealing how structural fluctuations may affect properties such as stability and phase transitions and provide insights into how MOFs deform under external stresses or during adsorption/desorption processes. On the other hand, by employing a stochastic approach, MC simulations can efficiently explore a wide range of configurations, making them well-suited for adsorption simulations to predict isotherms and heats of adsorption. Together, MD and MC simulations offer a comprehensive way to explore MOF behavior, encompassing both dynamic and equilibrium properties. By combining the strengths of these two methods, researchers can gain a more complete understanding of the mechanisms and phenomena occurring in MOF structures and hence design new materials with tailored properties for various applications.

Machine learning techniques are playing an increasing role in both quantum chemical and classical modeling, allowing high-accuracy predictions at reduced computational costs. Within the context of DFT, ML methods can predict oxidation and spin states. Additionally, ML techniques can monitor geometry optimizations to ensure convergence to meaningful resulting structures. Within the realm of classical simulations, ML methods can be employed to achieve high-accuracy interaction models through ML force fields and by predicting ab initio quality partial charges. Furthermore, these techniques can assist in screening databases to determine the water and thermal stability of MOFs and can be trained to predict other properties of interest.

As MOF research continues its rapid evolution, modeling and simulation strategies need to evolve in parallel. An important challenge is the inherent flexibility of MOFs, which is routinely overlooked or inadequately addressed in simulations, in particular in the field of adsorption. The importance of flexibility spans from small changes such as the lability of modulators and rotation of polar functional groups in zirconium MOFs, which can impact the strength of adsorption of small molecules, to the rotation of the linkers that might facilitate diffusion and packing of guest molecules. Larger-scale structural flexibility of MOFs, exemplified by phenomena such as breathing associated with significant volume changes, presents a challenge for standard adsorption simulation protocols. Within these challenges naturally lie opportunities. The immediate frontier is to integrate MOF flexibility within the simulation protocols. Classical force fields can be refined and expanded upon to better capture these dynamics. Moreover, with the advancement of ML techniques, there is a significant promise in developing universal ML potentials for MOFs that can account for framework flexibility and MOF-adsorbate reactivity with the accuracy of quantum methods. By leveraging such methodologies, and with the aid of modern computational advancements like GPU acceleration, there is potential to achieve an unprecedented level of accuracy in predicting MOF behavior under various conditions.

Over the past two decades, computational tools have played a pivotal role in MOF research, facilitating the rapid development and characterization of new MOF materials for specific applications. As we move forward, the next frontier for MOF modeling is not merely about refining simulations but delving deeper to understand the behavior of these materials under diverse conditions. The growing accessibility and reliability of computational methods, from density functional theory to Monte Carlo and molecular dynamics simulations, combined with the integration of novel ML techniques and advanced computational resources, are set to redefine the landscape of MOF research. Through this review, we aim to ease the transition of these computational modeling techniques into the toolkits of emerging researchers in the exciting field of MOF research.

Conflict of Interest

RQS has a financial interest in the startup company NuMat Technologies, which is commercializing metal-organic frameworks.

[1] H. Li, K. Wang, Y. Sun, C. T. Lollar, J. Li, H.-C. Zhou, *Mater. Today* **2018**, *21*, 108.

[2] J. A. Mason, M. Veenstra, J. R. Long, *Chem. Sci.* **2013**, *5*, 32.

[3] K. Sumida, D. L. Rogow, J. A. Mason, T. M. Mcdonald, E. D. Bloch, Z. R. Herm, T.-H. Bae, J. R. Long, *Chem. Rev.* **2012**, *112*, 724.

[4] M. P. Suh, H. J. Park, T. K. Prasad, D.-W. Lim, *Chem. Rev.* **2012**, *112*, 782.

[5] J.-R. Li, J. Sculley, H.-C. Zhou, *Chem. Rev.* **2012**, *112*, 869.

[6] A. Bavykina, N. Kolobov, I.l S. Khan, J. A. Bau, A. Ramirez, J. Gascon, *Chem. Rev.* **2020**, *120*, 8468.

[7] A. Corma, H. García, F. X. Llabrés I Xamena, *Chem. Rev.* **2010**, *110*, 4606.

[8] J. Jiang, O. M. Yaghi, *Chem. Rev.* **2015**, *115*, 6966.

[9] A. Iliescu, J. J. Oppenheim, C. Sun, M. Dinca, *Chem. Rev.* **2022**, *123*, 6197.

[10] J. F. Keggin, F. D. Miles, *Nature* **1936**, *137*, 577.

[11] S. R. Batten, N. R. Champness, X.-M. Chen, J. Garcia-Martinez, S. Kitagawa, L. Öhrström, M. O'keeffe, M. Paik Suh, J. Reedijk, *Pure Appl. Chem.* **2013**, *85*, 1715.

[12] B. F. Hoskins, R. Robson, *J. Am. Chem. Soc.* **1989**, *111*, 5962.

[13] M. Kondo, T. Yoshitomi, H. Matsuzaka, S. Kitagawa, K. Seki, *Angew. Chem., Int. Ed. Engl.* **1997**, *36*, 1725.

[14] O. M. Yaghi, H. Li, *J. Am. Chem. Soc.* **1995**, *117*, 10401.

[15] H. Li, M. Eddaoudi, M. O'keeffe, O. M. Yaghi, *Nature* **1999**, *402*, 276.

[16] N. L. Rosi, J. Eckert, M. Eddaoudi, D. T. Vodak, J. Kim, M. O'keeffe, O. M. Yaghi, *Science* **2003**, *300*, 1127.

[17] Y. G. Chung, E. Haldoupis, B. J. Bucior, M. Haranczyk, S. Lee, H. Zhang, K. D. Vogiatzis, M. Milisavljevic, S. Ling, J. S. Camp, B. Slater, J. I. Siepmann, D. S. Sholl, R. Q. Snurr, *J. Chem. Eng. Data* **2019**, *64*, 5985.

[18] Y. G. Chung, J. Camp, M. Haranczyk, B. J. Sikora, W. Bury, V. Krungleviciute, T. Yildirim, O. K. Farha, D. S. Sholl, R. Q. Snurr, *Chem. Mater.* **2014**, *26*, 6185.

[19] S. S.-Y. Chui, S. M.-F. Lo, J. P. H. Charmant, A. G. Orpen, I. D. Williams, *Science* **1999**, *283*, 1148.

[20] N. L. Rosi, J. Kim, M. Eddaoudi, B. Chen, M. O'keeffe, O. M. Yaghi, *J. Am. Chem. Soc.* **2005**, *127*, 1504.

[21] H. Deng, S. Grunder, K. E. Cordova, C. Valente, H. Furukawa, M. Hmadeh, F. Gándara, A. C. Whalley, Z. Liu, S. Asahina, H. Kazumori, M. O'keeffe, O. Terasaki, J. F. Stoddart, O. M. Yaghi, *Science* **2012**, *336*, 1018.

[22] F. Millange, C. Serre, G. Férey, *Sci. Rev. Chem. Commun.* **2002**, *2*, 822.

[23] T. Loiseau, C. Serre, C. Huguenard, G. Fink, F. Taulelle, M. Henry, T. Bataille, G. Férey, *Chemistry* **2004**, *10*, 1373.

[24] K. Barthelet, J. Marrot, D. Riou, G. Ferey, *Angew. Chem., Int. Ed.* **2002**, *41*, https://doi.org/10.1002/1521-3773.

[25] Y. Liu, J.-H. Her, A. Dailly, A. J. Ramirez-Cuesta, D. A. Neumann, C. M. Brown, *J. Am. Chem. Soc.* **2008**, *130*, 11813.

[26] X.-C. Huang, Y.-Y. Lin, J.-P. Zhang, X.-M. Chen, *Angew. Chem., Int. Ed.* **2006**, *45*, 1557.

[27] K. S. Park, Z. Ni, A. P. Côté, J. Y. Choi, R. Huang, F. J. Uribe-Romo, H. K. Chae, M. O'keeffe, O. M. Yaghi, *Proc. Natl. Acad. Sci. USA* **2006**, *103*, 10186.

[28] D. Fairen-Jimenez, S. A. Moggach, M. T. Wharmby, P. A. Wright, S. Parsons, T. Düren, *J. Am. Chem. Soc.* **2011**, *133*, 8900.

[29] S. A. Moggach, T. D. Bennett, A. K. Cheetham, *Angew. Chem., Int. Ed.* **2009**, *48*, 7087.

[30] J. H. Cavka, S. Jakobsen, U. Olsbye, N. Guillou, C. Lamberti, S. Bordiga, K. P. Lillerud, *J. Am. Chem. Soc.* **2008**, *130*, 13850.

[31] J. E. Mondloch, W. Bury, D. Fairen-Jimenez, S. Kwon, E. J. Demarco, M. H. Weston, A. A. Sarjeant, S. T. Nguyen, P. C. Stair, R. Q. Snurr, O. K. Farha, J. T. Hupp, *J. Am. Chem. Soc.* **2013**, *135*, 10294.

[32] Z. Lu, J. Liu, X. Zhang, Y. Liao, R. Wang, K. Zhang, J. Lyu, O. K. Farha, J. T. Hupp, *J. Am. Chem. Soc.* **2020**, *142*, 21110.

[33] J. E. Mondloch, M. J. Katz, W. C. Isley Iii, P. Ghosh, P. Liao, W. Bury, G. W. Wagner, M. G. Hall, J. B. Decoste, G. W. Peterson, R. Q. Snurr, C. J. Cramer, J. T. Hupp, O. K. Farha, *Nat. Mater.* **2015**, *14*, 512.

[34] H. Furukawa, F. Gándara, Y.-B. Zhang, J. Jiang, W. L. Queen, M. R. Hudson, O. M. Yaghi, *J. Am. Chem. Soc.* **2014**, *136*, 4369.

[35] D. Feng, Z.-Y. Gu, J.-R. Li, H.-L. Jiang, Z. Wei, H.-C. Zhou, *Angew. Chem.* **2012**, *124*, 10453.

[36] S. Krause, V. Bon, I. Senkovska, U. Stoeck, D. Wallacher, D. M. Többens, S. Zander, R. S. Pillai, G. Maurin, F.-X. Coudert, S. Kaskel, *Nature* **2016**, *532*, 348.

[37] U. Stoeck, S. Krause, V. Bon, I. Senkovska, S. Kaskel, *Chem. Commun.* **2012**, *48*, 10841.

[38] K. S. Walton, R. Q. Snurr, *J. Am. Chem. Soc.* **2007**, *129*, 8552.

[39] O. K. Farha, I. Eryazici, N. C. Jeong, B. G. Hauser, C. E. Wilmer, A. A. Sarjeant, R. Q. Snurr, S. T. Nguyen, A. Ö. Yazaydin, J. T. Hupp, *J. Am. Chem. Soc.* **2012**, *134*, 15016.

[40] I. M. Hönicke, I. Senkovska, V. Bon, I. A. Baburin, N. Bönisch, S. Raschke, J. D. Evans, S. Kaskel, *Angew. Chem., Int. Ed.* **2018**, *57*, 13780.

[41] J.-B. Lin, T. T. T. Nguyen, R. Vaidhyanathan, J. Burner, J. M. Taylor, H. Durekova, F. Akhtar, R. K. Mah, O. Ghaffari-Nik, S. Marx, N. Fylstra, S. S. Iremonger, K. W. Dawson, P. Sarkar, P. Hovington, A. Rajendran, T. K. Woo, G. K. H. Shimizu, *Science* **2021**, *374*, 1464.

[42] Pold87/academic-keyword-occurrence: Extracts the historic word occurrence of a search term in academic papers,

https://github.com/Pold87/academic-keyword-occurrence, (accessed: June 2023).

[43] T. Kawakami, S. Takamizawa, Y. Kitagawa, T. Maruta, W. Mori, K. Yamaguchi, *Polyhedron* **2001**, *20*, 1197.

[44] A. Vishnyakov, P. I. Ravikovitch, A. V. Neimark, M. Bülow, Q. M. Wang, *Nano Lett.* **2003**, *3*, 713.

[45] T. Sagara, J. Klassen, E. Ganz, *J. Chem. Phys.* **2004**, *121*, 12543.

[46] T. Düren, L. Sarkisov, O. M. Yaghi, R. Q. Snurr, *Langmuir* **2004**, *20*, 2683.

[47] L. Sarkisov, T. Düren, R. Q. Snurr, *Mol. Phys.* **2006**, *102*, 211.

[48] A. I. Skoulidas, D. S. Sholl, *J. Phys. Chem. B* **2005**, *109*, 15760.

[49] S. Keskin, D. S. Sholl, *Langmuir* **2009**, *25*, 11786.

[50] C. E. Wilmer, M. Leaf, C. Y. Lee, O. K. Farha, B. G. Hauser, J. T. Hupp, R. Q. Snurr, *Nat. Chem.* **2011**, *4*, 83.

[51] M. Fernandez, P. G. Boyd, T. D. Daff, M. Z. Aghaji, T. K. Woo, *J. Phys. Chem. Lett.* **2014**, *5*, 3056.

[52] K. M. Jablonka, D. Ongari, S. M. Moosavi, B. Smit, *Chem. Rev.* **2020**, *120*, 8066.

[53] P. Hohenberg, W. Kohn, *Phys. Rev.* **1964**, *136*, B864.

[54] W. Kohn, L. J. Sham, *Phys. Rev.* **1965**, *140*, A1133.

[55] M. Bursch, J.-M. Mewes, A. Hansen, S. Grimme, *Angew. Chem., Int. Ed.* **2022**, *61*, e202205735.

[56] A. R. Leach, *Molecular Modelling: Principles and Applications*, Longman, London **1996**.

[57] D. S. Sholl, J. A. Steckel, *Density Functional Theory: A Practical Introduction*, John Wiley and Sons, New York **2009**.

[58] D. Nazarian, P. Ganesh, D. S. Sholl, *J. Mater. Chem. A* **2015**, *3*, 22432.

[59] F. Formalik, M. Fischer, J. Rogacka, L. Firlej, B. Kuchta, *J. Chem. Phys.* **2018**, *149*, 064110.

[60] E. Caldeweyher, S. Ehlert, A. Hansen, H. Neugebauer, S. Spicher, C. Bannwarth, S. Grimme, *J. Chem. Phys.* **2019**, *150*, 154122.

[61] S. Grimme, S. Ehrlich, L. Goerigk, *J. Comput. Chem.* **2011**, *32*, 1456.

[62] S. Grimme, J. Antony, S. Ehrlich, H. Krieg, *J. Chem. Phys.* **2010**, *132*, 154104.

[63] S. Grimme, *J. Comput. Chem.* **2006**, *27*, 1787.

[64] A. Tkatchenko, M. Scheffler, *Phys. Rev. Lett.* **2009**, *102*, 073005.

[65] H. Peng, Z.-H. Yang, J. P. Perdew, J. Sun, *Phys. Rev. X* **2016**, *6*, 041005.

[66] J. Ning, M. Kothakonda, J. W. Furness, A. D. Kaplan, S. Ehlert, J. G. Brandenburg, J. P. Perdew, J. Sun, *Phys. Rev. B* **2022**, *106*, 075422.

[67] I. Hamada, *Phys. Rev. B: Condens. Matter Mater. Phys.* **2014**, *89*, 121103.

[68] K. Lee, É. D. Murray, L. Kong, B. I. Lundqvist, D. C. Langreth, *Phys. Rev. B: Condens. Matter Mater. Phys.* **2010**, *82*, 081101.

[69] M. Dion, H. Rydberg, E. Schröder, D. C. Langreth, B. I. Lundqvist, *Phys. Rev. Lett.* **2004**, *92*, 246401.

[70] M. R. Ryder, B. Civalleri, G. Cinque, J.-C. Tan, *CrystEngComm* **2016**, *18*, 4303.

[71] M. R. Ryder, B. Civalleri, T. Bennett, S. Henke, S. Rudic, G. Cinque, F. Fernandez-Alonso, J.-C. Tan, *Phys. Rev. Lett.* **2014**, *113*, 215502.

[72] N. Y. Tan, M. T. Ruggiero, C. Orellana-Tavra, T. Tian, A. D. Bond, T. M. Korter, D. Fairen-Jimenez, J. Axel Zeitler, *Chem. Commun.* **2015**, *51*, 16037.

[73] F. Formalik, B. Mazur, M. Fischer, L. Firlej, B. Kuchta, *J. Phys. Chem. C* **2021**, *125*, 7999.

[74] F. Formalik, M. Fischer, J. Rogacka, L. Firlej, B. Kuchta, *Microporous Mesoporous Mater.* **2020**, *304*, 109132.

[75] A. E. J. Hoffman, L. Vanduyfhuys, I. Nevjestic, J. Wieme, S. M. J. Rogge, H. Depauw, P. Van Der Voort, H. Vrielinck, V. Van Speybroeck, *J. Phys. Chem. C* **2018**, *122*, 2734.

[76] A. E. J. Hoffman, I. Senkovska, J. Wieme, A. Krylov, S. Kaskel, V. Van Speybroeck, *J. Mater. Chem. A* **2022**, *10*, 17254.

[77] W. Zhang, J. Maul, D. Vulpe, P. Z. Moghadam, D. Fairen-Jimenez, D. M. Mittleman, J. A. Zeitler, A. Erba, M. T. Ruggiero, *J. Phys. Chem. C* **2018**, *122*, 27442.

**ADVANCED
SCIENCE NEWS**

www.advancedsciencenews.com

**ADVANCED
FUNCTIONAL
MATERIALS**

www.afm-journal.de

[78] L. H. N. Rimmer, M. T. Dove, A. L. Goodwin, D. C. Palmer, *Phys. Chem. Chem. Phys.* **2014**, *16*, 21144.

[79] P. Iacomi, F. Formalik, J. Marreiros, J. Shang, J. Rogacka, A. Mohmeyer, P. Behrens, R. Ameloot, B. Kuchta, P. L. Llewellyn, *Chem. Mater.* **2019**, *31*, 8413.

[80] B. Zheng, Y. Zhu, F. Fu, L. L.i Wang, J. Wang, H. Du, *RSC Adv.* **2017**, *7*, 41499.

[81] M. R. Ryder, J.-C. Tan, *Dalton Trans.* **2016**, *45*, 4154.

[82] A. E. J. Hoffman, J. Wieme, S. M. J. Rogge, L. Vanduyfhuys, V. Van Speybroeck, *Z. Kristallogr. - Cryst. Mater* **2019**, *234*, 529.

[83] E. Cockayne, *J. Phys. Chem. C* **2017**, *121*, 4312.

[84] F. Formalik, A. V. Neimark, J. Rogacka, L. Firlej, B. Kuchta, *J. Colloid Interface Sci.* **2020**, *578*, 77.

[85] J. D. Evans, L. Bocquet, F.-X. Coudert, *Chem* **2016**, *1*, 873.

[86] K. Roztocki, F. Formalik, A. Krawczuk, I. Senkovska, B. Kuchta, S. Kaskel, D. Matoga, *Angew. Chem., Int. Ed.* **2020**, *59*, 4491.

[87] P. Iacomi, J.i S. Lee, L. Vanduyfhuys, K. H.o Cho, P. Fertey, J. Wieme, D. Granier, G. Maurin, V. Van Speybroeck, J.-S. Chang, P. G. Yot, *Chem. Sci.* **2021**, *12*, 5682.

[88] L. Chaput, A. Togo, I. Tanaka, G. Hug, *Phys. Rev. B: Condens. Matter Mater. Phys.* **2011**, *84*, 094302.

[89] A. Togo, L. Chaput, I. Tanaka, G. Hug, *Phys. Rev. B: Condens. Matter Mater. Phys.* **2010**, *81*, 174301.

[90] T. G. Grissom, D. M. Driscoll, D. Troya, N. S. Sapienza, P. M. Usov, A. J. Morris, J. R. Morris, *J. Phys. Chem. C* **2019**, *123*, 13731.

[91] T. M. Rayder, F. Formalik, S. M. Vornholt, H. Frank, S. Lee, M. Alzayer, Z. Chen, D. Sengupta, T. Islamoglu, F. Paesani, K. W. Chapman, R. Q. Snurr, O. K. Farha, *J. Am. Chem. Soc.* **2023**, *145*, 11195.

[92] K. Tan, H. Pandey, H. Wang, E. Velasco, K.-Y.u Wang, H.-C. Zhou, J. Li, T. Thonhauser, *J. Am. Chem. Soc.* **2021**, *143*, 6328.

[93] Database of Frequency Scale Factors for Electronic Model Chemistries, https://comp.chem.umn.edu/freqscale/ (accessed: March, 2023).

[94] I. M. Alecu, J. Zheng, Y. Zhao, D. G. Truhlar, *J. Chem. Theory Comput.* **2010**, *6*, 2872.

[95] S. Grimme, *Chemistry* **2012**, *18*, 9955.

[96] Y.i-P. Li, J. Gomes, S. Mallikarjun Sharada, A. T. Bell, M. Head-Gordon, *J. Phys. Chem. C* **2015**, *119*, 1840.

[97] M. Mammen, E. I. Shakhnovich, J. M. Deutch, G. M. Whitesides, *J. Org. Chem.* **1998**, *63*, 3821.

[98] G. Luchini, J. V. Alegre-Requena, I. Funes-Ardoiz, R. S. Paton, *F1000Research* **2020**, *9*, 291.

[99] H. Chen, P. Liao, M. L. Mendonca, R. Q. Snurr, *J. Phys. Chem. C* **2018**, *122*, 12362.

[100] G. Henkelman, B. P. Uberuaga, H. Jónsson, *J. Chem. Phys.* **2000**, *113*, 9901.

[101] D. Sheppard, P. Xiao, W. Chemelewski, D. D. Johnson, G. Henkelman, *J. Chem. Phys.* **2012**, *136*, 74103.

[102] G. Henkelman, H. Jónsson, *J. Chem. Phys.* **2000**, *113*, 9978.

[103] J. Kästner, P. Sherwood, *J. Chem. Phys.* **2008**, *128*, 14106.

[104] G. Henkelman, H. Jónsson, *J. Chem. Phys.* **1999**, *111*, 7010.

[105] H. B. Schlegel, *J. Comput. Chem.* **1982**, *3*, 214.

[106] A. S. Rosen, J. M. Notestein, R. Q. Snurr, *Phys. Chem. Chem. Phys.* **2022**, *24*, 8129.

[107] A. Nandy, C. Duan, C. Goffinet, H. J. Kulik, *JACS Au* **2022**, *2*, 1200.

[108] A. S. Rosen, J. M. Notestein, R. Q. Snurr, *ACS Catal.* **2019**, *9*, 3576.

[109] T. Ikuno, J. Zheng, A. Vjunov, M. Sanchez-Sanchez, M. A. Ortuño, D. R. Pahls, J. L. Fulton, D. M. Camaioni, Z. Li, D. Ray, B. L. Mehdi, N. D. Browning, O. K. Farha, J. T. Hupp, C. J. Cramer, L. Gagliardi, J. A. Lercher, *J. Am. Chem. Soc.* **2017**, *139*, 10294.

[110] J. G. Vitillo, A. Bhan, C. J. Cramer, C. C. Lu, L. Gagliardi, *ACS Catal.* **2019**, *9*, 2870.

[111] D. R. Pahls, M. A. Ortuño, P. H. Winegar, C. J. Cramer, L. Gagliardi, *Inorg. Chem.* **2017**, *56*, 8739.

[112] M. C. Simons, S. D. Prinslow, M. Babucci, A. S. Hoffman, J. Hong, J. G. Vitillo, S. R. Bare, B. C. Gates, C. C. Lu, L. Gagliardi, A. Bhan, *J. Am. Chem. Soc.* **2021**, *143*, 12165.

[113] J. G. Vitillo, C. C. Lu, C. J. Cramer, A. Bhan, L. Gagliardi, *ACS Catal.* **2021**, *11*, 579.

[114] M. Barona, S. Ahn, W. Morris, W. Hoover, J. M. Notestein, O. K. Farha, R. Q. Snurr, *ACS Catal.* **2020**, *10*, 1460.

[115] K. D. Vogiatzis, E. Haldoupis, D. J. Xiao, J. R. Long, J. I. Siepmann, L. Gagliardi, *J. Phys. Chem. C* **2016**, *120*, 18707.

[116] M. Barona, R. Q. Snurr, *ACS Appl. Mater. Interfaces* **2020**, *12*, 28217.

[117] X. Wu, L. Chen, E. J. Amigues, R. Wang, Z. Pang, L. Ding, *ACS Omega* **2021**, *6*, 18169.

[118] M. R. Mian, X. Wang, X. Wang, K. O. Kirlikovali, H. Xie, K. Ma, K. M. Fahy, H. Chen, T. Islamoglu, R. Q. Snurr, O. K. Farha, *J. Am. Chem. Soc.* **2023**, *145*, 7435.

[119] G. Mínguez Espallargas, E. Coronado, *Chem. Soc. Rev.* **2018**, *47*, 533.

[120] B.o Yang, X.-P. Wu, L. Gagliardi, D. G. Truhlar, *J. Phys. Chem. B* **2021**, *125*, 5786.

[121] A. Nandy, H. Adamji, D. W. Kastner, V. Vennelakanti, A. Nazemi, M. Liu, H. J. Kulik, *ACS Catal.* **2022**, *12*, 9281.

[122] J. Hubbard, *Proc. R. Soc. London, Ser. A* **1963**, *276*, 238.

[123] A. S. Rosen, J. M. Notestein, R. Q. Snurr, *J. Chem. Phys.* **2020**, *152*, 224101.

[124] T. Z. H. Gani, H. J. Kulik, *J. Chem. Theory Comput.* **2016**, *12*, 5931.

[125] M. Cossi, V. Barone, R. Cammi, J. Tomasi, *Chem. Phys. Lett.* **1996**, *255*, 327.

[126] L. Vanduyfhuys, S. Vandenbrande, T. Verstraelen, R. Schmid, M. Waroquier, V. Van Speybroeck, *J. Comput. Chem.* **2015**, *36*, 1015.

[127] L. Vanduyfhuys, S. Vandenbrande, J. Wieme, M. Waroquier, T. Verstraelen, V. Van Speybroeck, *J. Comput. Chem.* **2018**, *39*, 999.

[128] S. Borgmans, S. M. J. Rogge, J. S. De Vos, P. Van Der Voort, V. Van Speybroeck, *Commun Chem* **2023**, *6*, 5.

[129] S. M. J. Rogge, S. Borgmans, V. Van Speybroeck, *Matter* **2023**, *6*, 1435.

[130] T. A. Manz, D. S. Sholl, *J. Chem. Theory Comput.* **2010**, *6*, 2455.

[131] N. G. Limas, T. A. Manz, *RSC Adv.* **2018**, *8*, 2678.

[132] T. A. Manz, *RSC Adv.* **2017**, *7*, 45552.

[133] N. G. Limas, T. A. Manz, *RSC Adv.* **2016**, *6*, 45727.

[134] T. A. Manz, N. G. Limas, *RSC Adv.* **2016**, *6*, 47771.

[135] C. Campañá, B. Mussard, T. K. Woo, *J. Chem. Theory Comput.* **2009**, *5*, 2866.

[136] S. Liu, B. Luan, *Nanoscale* **2022**, *14*, 9466.

[137] C. Duan, A. Nandy, R. Meyer, N. Arunachalam, H. J. Kulik, *Nat. Comput. Sci.* **2022**, *3*, 38.

[138] C. Riplinger, F. Neese, *J. Chem. Phys.* **2013**, *138*, 034106.

[139] M. G. Taylor, T. Yang, S. Lin, A. Nandy, J. P. Janet, C. Duan, H. J. Kulik, *J. Phys. Chem. A* **2020**, *124*, 3286.

[140] oxiMACHINE, (n.d.). https://oximachine.materialscloud.io/ (accessed: April 2023).

[141] K. M. Jablonka, D. Ongari, S. M. Moosavi, B. Smit, *Nat. Chem.* **2021**, *13*, 771.

[142] C. Duan, A. Nandy, H. Adamji, Y. Roman-Leshkov, H. J. Kulik, *J. Chem. Theory Comput.* **2022**, *18*, 4282.

[143] S. M. Moosavi, B. Á. Novotny, D. Ongari, E. Moubarak, M. Asgari, Ö. Kadioglu, C. Charalambous, A. Ortega-Guerrero, A. H. Farmahini, L. Sarkisov, S. Garcia, F. Noé, B. Smit, *Nat. Mater.* **2022**, *21*, 1419.

[144] A. S. Rosen, S. M. Iyer, D. Ray, Z. Yao, A. Aspuru-Guzik, L. Gagliardi, J. M. Notestein, R. Q. Snurr, *Matter* **2021**, *4*, 1578.

[145] P. Z. Moghadam, S. M. J. Rogge, A. Li, C.-M. Chow, J. Wieme, N. Moharrami, M. Aragones-Anglada, G. Conduit, D. A. Gomez-Gualdron, V. Van Speybroeck, D. Fairen-Jimenez, *Matter* **2019**, *1*, 219.

[146] D. J. Adams, *Mol. Phys.* **1974**, *29*, 307.

[147] G. E. Norman, V. S. Filinov, *High Temp.* **1969**, *7*, 216.

[148] A. Z. Panagiotopoulos, N. Quirke, M. Stapleton, D. J. Tildesley, *Mol. Phys.* **2007**, *63*, 527.

[149] N. Metropolis, A. W. Rosenbluth, M. N. Rosenbluth, A. H. Teller, E. Teller, *J. Chem. Phys.* **1953**, *21*, 1087.

[150] D. Frenkel, B. Smit, *Understanding Molecular Simulation*, 2nd ed., Academic Press, Inc., Academic San Diego, CA **2002**.

[151] H. Furukawa, N. Ko, Y. B. Go, N. Aratani, S. B. Choi, E. Choi, A. Ö. Yazaydin, R. Q. Snurr, M. O'keeffe, J. Kim, O. M. Yaghi, *Science* **2010**, *329*, 424.

[152] L. Sarkisov, *Dalton Trans.* **2016**, *45*, 4203.

[153] N. Hanikel, D. Kurandina, S. Chheda, Z. Zheng, Z. Rong, S. E. Neumann, J. Sauer, J. I. Siepmann, L. Gagliardi, O. M. Yaghi, *ACS Cent. Sci.* **2023**, *9*, 551.

[154] D.-Y.u Peng, D. B. Robinson, *Ind. Eng. Chem. Fundam.* **1976**, *15*, 59.

[155] D. Dubbeldam, A. Torres-Knoop, K. S. Walton, *Mol. Simul.* **2013**, *39*, 1253.

[156] M. P. Allen, D. J. Tildesley, *Computer Simulation of Liquids*, 2nd ed., Oxford University Press, Oxford, UK **2017**.

[157] D. Dubbeldam, S. Calero, D. E. Ellis, R. Q. Snurr, *Mol. Simul.* **2016**, *42*, 81.

[158] J. A. Purton, J. C. Crabtree, S. C. Parker, *Mol. Simul.* **2013**, *39*, 1240.

[159] J. K. Shah, E. Marin-Rimoldi, R. G. Mullen, B. P. Keene, S. Khan, A. S. Paluch, N. Rai, L. L. Romanielo, T. W. Rosch, B. Yoo, E. J. Maginn, *J. Comput. Chem.* **2017**, *38*, 1727.

[160] M. G. Martin, *Mol. Simul.* **2013**, *39*, 1212.

[161] Y. Nejahi, M. Soroush Barhaghi, J. Mick, B. Jackman, K. Rushaidat, Y. Li, L. Schwiebert, J. Potoff, *SoftwareX* **2019**, *9*, 20.

[162] A. P. Thompson, H. M. Aktulga, R. Berger, D. S. Bolintineanu, W. M. Brown, P. S. Crozier, P. J. In 'T Veld, A. Kohlmeyer, S. G. Moore, T. D. Nguyen, R. Shan, M. J. Stevens, J. Tranchida, C. Trott, S. J. Plimpton, *Comput. Phys. Commun.* **2022**, *271*, 108171.

[163] J. C. Phillips, D. J. Hardy, J. D. C. Maia, J. E. Stone, J. V. Ribeiro, R. C. Bernardi, R. Buch, G. Fiorin, J. Hénin, W. Jiang, R. Mcgreevy, M. C. R. Melo, B. K. Radak, R. D. Skeel, A. Singharoy, Y.i Wang, B. Roux, A. Aksimentiev, Z. Luthey-Schulten, L. V. Kalé, K. Schulten, C. Chipot, E. Tajkhorshid, *J. Chem. Phys.* **2020**, *153*, 44130.

[164] M. J. Abraham, T. Murtola, R. Schulz, S. Páll, J. C. Smith, B. Hess, E. Lindahl, *SoftwareX* **2015**, *1-2*, 19.

[165] J. A. Anderson, J. Glaser, S. C. Glotzer, *Comput. Mater. Sci.* **2020**, *173*, 109363.

[166] S. M. J. Rogge, R. Goeminne, R. Demuynck, J. J. Gutiérrez-Sevillano, S. Vandenbrande, L. Vanduyfhuys, M. Waroquier, T. Verstraelen, V. Van Speybroeck, *Adv Theory Simul* **2019**, *2*, 1800177.

[167] D. N. Theodorou, R. Q. Snurr, A. T. Bell, in *Comprehensive Supramolecular Chemistry*, Vol. *7*, (Eds: G. Alberti, T. Bein) Pergamon, Oxford, **1996**, pp. 507–548.

[168] C. H. Sharp, B. C. Bukowski, H. Li, E. M. Johnson, S. Ilic, A. J. Morris, D. Gersappe, R. Q. Snurr, J. R. Morris, *Chem. Soc. Rev.* **2021**, *50*, 11530.

[169] H. Xu, R. Cabriolu, B. Smit, *J. Chem. Theory Comput.* **2022**, *18*, 2826.

[170] R. Wang, K. Shi, J. Liu, R. Q. Snurr, J. T. Hupp, *J. Am. Chem. Soc.* **2023**, *145*, 13979.

[171] B. C. Bukowski, R. Q. Snurr, *ACS Appl. Mater. Interfaces* **2020**, *12*, 56049.

[172] B. C. Bukowski, R. Q. Snurr, *ACS Appl. Mater. Interfaces* **2022**, *14*, 55608.

[173] H. Babaei, P. Keblinski, J. M. Khodadadi, *J. Appl. Phys.* **2012**, *112*, 54310.

[174] P. K. Schelling, S. R. Phillpot, P. Keblinski, *Phys. Rev. B* **2002**, *65*, 144306.

[175] M. S. Green, *J. Chem. Phys.* **1954**, *22*, 398.

[176] B. L. Huang, A. J. H. Mcgaughey, M. Kaviany, *Int. J. Heat Mass Transfer* **2007**, *50*, 393.

[177] H. Babaei, A. J. H. Mcgaughey, C. E. Wilmer, *Chem. Sci.* **2016**, *8*, 583.

[178] M. Islamov, H. Babaei, R. Anderson, K. B. Sezginel, J. R. Long, A. J. H. Mcgaughey, D. A. Gomez-Gualdron, C. E. Wilmer, *npj Comput. Mater.* **2023**, *9*, 11.

[179] K. B. Sezginel, S. Lee, H. Babaei, C. E. Wilmer, *J. Phys. Chem. C* **2020**, *124*, 18604.

[180] E. Braun, J. Gilmer, H. B. Mayes, D. L. Mobley, J. I. Monroe, S. Prasad, D. M. Zuckerman, *Living J. Comput. Mol. Sci.* **2019**, *1*, 5957.

[181] N. Planas, J. E. Mondloch, S. Tussupbayev, J. Borycz, L. Gagliardi, J. T. Hupp, O. K. Farha, C. J. Cramer, *J. Phys. Chem. Lett.* **2014**, *5*, 3716.

[182] T. Chen, T. A. Manz, *RSC Adv.* **2020**, *10*, 26944.

[183] M. A. Addicoat, D. E. Coupry, T. Heine, *J. Phys. Chem. A* **2014**, *118*, 9607.

[184] Y. J. Colón, D. A. Gómez-Gualdrón, R. Q. Snurr, *Cryst. Growth Des.* **2017**, *17*, 5801.

[185] R. Anderson, D. A. Gómez-Gualdrón, *CrystEngComm* **2019**, *21*, 1653.

[186] P. G. Boyd, T. K. Woo, *CrystEngComm* **2016**, *18*, 3777.

[187] S. Lee, B. Kim, H. Cho, H. Lee, S. Y. Lee, E. S. Cho, J. Kim, *ACS Appl. Mater. Interfaces* **2021**, *13*, 23647.

[188] A. K. Rappe, C. J. Casewit, K. S. Colwell, W. A. Goddard, W. M. Skiff, *J. Am. Chem. Soc.* **1992**, *114*, 10024.

[189] P. Z. Moghadam, A. Li, S. B. Wiggin, A. Tao, A. G. P. Maloney, P. A. Wood, S. C. Ward, D. Fairen-Jimenez, *Chem. Mater.* **2017**, *29*, 2618.

[190] S. Li, Y. G. Chung, C. M. Simon, R. Q. Snurr, *J. Phys. Chem. Lett.* **2017**, *8*, 6135.

[191] P. G. Boyd, A. Chidambaram, E. García-Díez, C. P. Ireland, T. D. Daff, R. Bounds, A. Gladysiak, P. Schouwink, S. M. Moosavi, M. M. Maroto-Valer, J. A. Reimer, J. A. R. Navarro, T. K. Woo, S. Garcia, K. C. Stylianou, B. Smit, *Nature* **2019**, *576*, 253.

[192] Y. Lan, T. Yan, M. Tong, C. Zhong, *J. Mater. Chem. A* **2019**, *7*, 12556.

[193] S. Majumdar, S. M. Moosavi, K. M. Jablonka, D. Ongari, B. Smit, *ACS Appl. Mater. Interfaces* **2021**, *13*, 61004.

[194] A. Nandy, S. Yue, C. Oh, C. Duan, G. G. Terrones, Y. G. Chung, H. J. Kulik, *Matter* **2023**, *6*, 1585.

[195] D. Dubbeldam, K. S. Walton, T. J. H. Vlugt, S. Calero, *Adv. Theory Simul.* **2019**, *2*, 1900135.

[196] B. L. Eggimann, A. J. Sunnarborg, H. D. Stern, A. P. Bliss, J. I. Siepmann, *Mol. Simul.* **2013**, *40*, 101.

[197] S. L. Mayo, B. D. Olafson, W. A. Goddard, *J. Phys. Chem.* **1990**, *94*, 8897.

[198] S. Vandenbrande, T. Verstraelen, J. J. Gutiérrez-Sevillano, M. Waroquier, V. Van Speybroeck, *J. Phys. Chem. C* **2017**, *121*, 25309.

[199] T. Verstraelen, S. Vandenbrande, F. Heidar-Zadeh, L. Vanduyfhuys, V. Van Speybroeck, M. Waroquier, P. W. Ayers, *J. Chem. Theory Comput.* **2016**, *12*, 3894.

[200] J. G. Mcdaniel, J. R. Schmidt, *J. Phys. Chem. C* **2012**, *116*, 14031.

[201] J. G. Mcdaniel, J. R. Schmidt, *J. Phys. Chem. A* **2013**, *117*, 2053.

[202] S. Vandenbrande, M. Waroquier, V. V. Speybroeck, T. Verstraelen, *J. Chem. Theory Comput.* **2017**, *13*, 161.

[203] N. S. Bobbitt, K. Shi, B. J. Bucior, H. Chen, N. Tracy-Amoroso, Z. Li, Y. Sun, J. H. Merlin, J. I. Siepmann, D. W. Siderius, R. Q. Snurr, *J. Chem. Eng. Data* **2023**, *68*, 483.

[204] A. K. Rappe, W. A. Goddard, *J. Phys. Chem.* **1991**, *95*, 3358.

[205] C. E. Wilmer, K.i C. Kim, R. Q. Snurr, *J. Phys. Chem. Lett.* **2012**, *3*, 2506.

[206] E. S. Kadantsev, P. G. Boyd, T. D. Daff, T. K. Woo, *J. Phys. Chem. Lett.* **2013**, *4*, 3056.

[207] D. Ongari, P. G. Boyd, O. Kadioglu, A. K. Mace, S. Keskin, B. Smit, *J. Chem. Theory Comput.* **2019**, *15*, 382.

[208] K. M. Jablonka, D. Ongari, B. Smit, *J. Chem. Theory Comput.* **2019**, *15*, 5635.

ADVANCED
SCIENCE NEWS

www.advancedsciencenews.com

ADVANCED
FUNCTIONAL
MATERIALS

www.afm-journal.de

[209] D. Dubbeldam, S. Calero, T. J. H. Vlugt, R. Krishna, T. L. M. Maesen, B. Smit, *J. Phys. Chem. B* **2004**, *108*, 12301.

[210] D. E. Coupry, M. A. Addicoat, T. Heine, *J. Chem. Theory Comput.* **2016**, *12*, 5215.

[211] Z. Hu, L. Zhang, J. Jiang, *J. Chem. Phys.* **2012**, *136*, 244703.

[212] J. A. Greathouse, M. D. Allendorf, *J. Phys. Chem. C* **2008**, *112*, 5795.

[213] Q. Yang, A. D. Wiersum, H. Jobic, V. Guillerm, C. Serre, P. L. Llewellyn, G. Maurin, *J. Phys. Chem. C* **2011**, *115*, 13768.

[214] E. Pantatosaki, G. Megariotis, A.-K. Pusch, C. Chmelik, F. Stallmach, G. K. Papadopoulos, *J. Phys. Chem. C* **2012**, *116*, 201.

[215] L. Zhang, G. Wu, J. Jiang, *J. Phys. Chem. C* **2014**, *118*, 8788.

[216] R. J. Verploegh, S. Nair, D. S. Sholl, *J. Am. Chem. Soc.* **2015**, *137*, 15760.

[217] B. Zheng, Y. Pan, Z. Lai, K.-W. Huang, *Langmuir* **2013**, *29*, 8865.

[218] P. Krokidas, S. Moncho, E. N. Brothers, I. G. Economou, *ACS Appl. Mater. Interfaces* **2020**, *12*, 20536.

[219] P. Krokidas, M. Castier, S. Moncho, E. Brothers, I. G. Economou, *J. Phys. Chem. C* **2015**, *119*, 27028.

[220] P. Krokidas, M. Castier, S. Moncho, D. N. Sredojevic, E. N. Brothers, H. T. Kwon, H.-K. Jeong, J. S. Lee, I. G. Economou, *J. Phys. Chem. C* **2016**, *120*, 8116.

[221] P. Krokidas, M. Castier, I. G. Economou, *J. Phys. Chem. C* **2017**, *121*, 17999.

[222] Y. Yang, D. S. Sholl, *J. Mater. Chem. A* **2022**, *10*, 4242.

[223] P. Krokidas, S. Karozis, S. Moncho, G. Giannakopoulos, E. N. Brothers, M. E. Kainourgiakis, I. G. Economou, T. A. Steriotis, *J. Mater. Chem. A* **2022**, *10*, 13697.

[224] P. G. Yot, Q. Ma, J. Haines, Q. Yang, A. Ghoufi, T. Devic, C. Serre, V. Dmitriev, G. Férey, C. Zhong, G. Maurin, *Chem. Sci.* **2012**, *3*, 1100.

[225] S. Jawahery, C. M. Simon, E. Braun, M. Witman, D. Tiana, B. Vlaisavljevich, B. Smit, *Nat. Commun.* **2017**, *8*, 13945.

[226] F. Salles, A. Ghoufi, G. Maurin, R. G. Bell, C. Mellot-Draznieks, G. Férey, *Angew. Chem., Int. Ed.* **2008**, *47*, 8487.

[227] J. K. Bristow, J. M. Skelton, K. L. Svane, A. Walsh, J. D. Gale, *Phys. Chem. Chem. Phys.* **2016**, *18*, 29316.

[228] J. Behler, M. Parrinello, *Phys. Rev. Lett.* **2007**, *98*, 146401.

[229] A. P. Bartók, M. C. Payne, R. Kondor, G. Csányi, *Phys. Rev. Lett.* **2010**, *104*, 136403.

[230] S. K. Achar, J. J. Wardzala, L. Bernasconi, L. Zhang, J. K. Johnson, *J. Chem. Theory Comput.* **2022**, *18*, 3593.

[231] S. Vandenhaute, M. Cools-Ceuppens, S. Dekeyser, T. Verstraelen, V. Van Speybroeck, *npj Comput. Mater.* **2023**, *9*, 19.

[232] C.-T.a Yang, I. Pandey, D. Trinh, C.-C. Chen, J. D. Howe, L.-C. Lin, *Mater. Adv.* **2022**, *3*, 5299.

[233] L.i-C. Lin, K. Lee, L. Gagliardi, J. B. Neaton, B. Smit, *J. Chem. Theory Comput.* **2014**, *10*, 1477.

[234] S. Yue, M. C. Muniz, M. F. Calegari Andrade, L. Zhang, R. Car, A. Z. Panagiotopoulos, *J. Chem. Phys.* **2021**, *154*, 34111.

[235] D. M. Anstine, O. Isayev, *J. Phys. Chem. A* **2023**, *127*, 2417.

[236] J. S. Smith, O. Isayev, A. E. Roitberg, *Chem. Sci.* **2017**, *8*, 3192.

[237] C. Chen, W. Ye, Y. Zuo, C. Zheng, S. P. Ong, *Chem. Mater.* **2019**, *31*, 3564.

[238] C. Chen, S. P. Ong, *Nat. Comput. Sci.* **2022**, *2*, 718.

[239] B. Deng, P. Zhong, K. Jun, K. Riebesell, K. Han, C. J. Bartel, G. Ceder, *Nat. Mach. Intell.* **2023**, *5*, 1031.

[240] Z. Yu, S. Jamdade, X. Yu, X. Cai, D. S. Sholl, *J. Phys. Chem. Lett.* **2023**, *14*, 6658.

[241] M. A. Addicoat, N. Vankova, I. F. Akter, T. Heine, *J. Chem. Theory Comput.* **2014**, *10*, 880.

[242] S. Wieser, E. Zojer, Machine learned Force-Fields for an ab-initio Quality Description of Metal-Organic Frameworks, https://arxiv.org/abs/2308.01278v2 (accessed: August 2023).

[243] C. Zou, D. R. Penley, E. H. Cho, L.-C. Lin, *J. Phys. Chem. C* **2020**, *124*, 11428.

[244] Q. Xu, C. Zhong, *J. Phys. Chem. C* **2010**, *114*, 5035.

[245] A. Raza, A. Sturluson, C. M. Simon, X. Fern, *J. Phys. Chem. C* **2020**, *124*, 19070.

[246] S. Kancharlapalli, A. Gopalan, M. Haranczyk, R. Q. Snurr, *J. Chem. Theory Comput.* **2021**, *17*, 3052.

[247] F. L. Oliveira, C. Cleeton, R. Neumann Barros Ferreira, B. Luan, A. H. Farmahini, L. Sarkisov, M. Steiner, *Sci Data* **2023**, *10*, 230.

[248] J. Burner, J. Luo, A. White, A. Mirmiran, O. Kwon, P. G. Boyd, S. Maley, M. Gibaldi, S. Simrod, V. Ogden, T. K. Woo, *Chem. Mater.* **2023**, *35*, 900.

Filip Formalik, born in Poland in 1992, started his academic journey at Wroclaw University of Science and Technology, earning an M.Sc. in physics (2016) and a Ph.D. in materials chemistry (2020) under the guidance of Prof. Bogdan Kuchta and Prof. Lucyna Firlej. In 2021, he received a Scholarship for Outstanding Young Scientists from the Minister of Science and Higher Education of the Republic of Poland. Since 2022 he has worked as a postdoctoral scholar in the Department of Chemical and Biological Engineering at Northwestern University with Prof. Randall Q. Snurr. In his research, he investigates the properties of porous materials, specifically focusing on adsorption and flexibility, using molecular modeling methods.

**ADVANCED
SCIENCE NEWS**

www.advancedsciencenews.com

**ADVANCED
FUNCTIONAL
MATERIALS**

www.afm-journal.de

Kaihang Shi received his Ph.D. in chemical engineering in 2020 from North Carolina State University, under the guidance of Profs. Keith Gubbins and Erik Santiso. After postdoctoral research at Northwestern University with Prof. Randall Snurr, in 2023, he joined the Department of Chemical and Biological Engineering at the University at Buffalo as an assistant professor. His research interests include computational modeling and machine learning of molecular adsorption, transport, and reaction in porous media, with an emphasis on materials design and characterization.

Faramarz Joodaki has been a postdoctoral scholar in Professor Randall Q. Snurr's Research Group in the Chemical and Biological Engineering Department of Northwestern University since 2020. He received his Ph.D. in chemical engineering under the supervision of Professor Michael L. Greenfield at the University of Rhode Island in 2020. His research interests are molecular modeling, theoretical computation, and vibrational analysis within material science, biophysics, and biochemistry.

Xijun Wang is a postdoctoral scholar at Northwestern University under Prof. Randall Q. Snurr, having earned his Ph.D. from the University of Science and Technology of China in 2017 with Prof. Jun Jiang. He was an exchange student at UC Santa Barbara from 2015 to 2016 with Prof. Baron G. Peters and later worked as a postdoc at North Carolina State University from 2019 to 2021 with Prof. Fanxing Li. His research centers on computational catalysis, targeting global challenges such as CO_2 capture, electrocatalytic ORR/OER, and the selective conversion of hydrocarbons. Additionally, he is using AI in chemistry to design state-of-the-art materials and catalysts.

Randall Q. Snurr is the John G. Searle Professor of Chemical and Biological Engineering at Northwestern University. He received his Ph.D. in chemical engineering from the University of California, Berkeley, and performed post-doctoral research at the University of Leipzig supported by an Alexander von Humboldt fellowship. Other honors include the Institute Award for Excellence in Industrial Gases Technology from AIChE and election as a corresponding member of the Saxon Academy of Sciences. His research interests include development of new nanoporous materials for solving energy and sustainability problems, molecular simulation, machine learning, adsorption separations, diffusion in nanoporous materials, and catalysis.

2308130 (25 of 25)